We thank both reviewers for their comments. Below we respond to all individual reviewer comments. Reviewer comments are denoted by italicized text.

Reviewer 1

1 Overview:

Lunt et al. present an analysis using 7 years of GOSAT methane measurements over Africa. They use these measurements in a hierarchical Bayesian inference framework to estimate monthly methane emissions from Africa. The authors then employ a number of correlative measurements (e.g., land surface temperature and water levels in Lake Victoria) to deduce the underlying drivers of these methane emissions. Overall, I think the work is excellent. The text is clear and reasonably concise, figures are generally high quality, and my comments are all seemingly minor. I suggest the paper be accepted pending minor revisions.

We thank the Reviewer for their assessment of the work and address their specific comments below.

2 Minor Comments:

2.1 Bias correction term for the model or GOSAT?

The only true shortcoming I found in the paper was the lack of a bias correction term. Most papers using GOSAT data have investigated the possibility of a latitudinally dependent bias. Fraser et al. (2014), Alexe et al. (2015), and Turner et al. (2015) all included some sort of polynomial or quadratic bias correction term (although some attributed it to the model stratosphere). Others used a bias term that was dependent on air mass factor (Cressot et al., 2014), that would also lead to latitudinal differences. The authors study domain covers ∼50◦of latitude, so it seems like this could be an important factor. Including this in the hierarchical inversion framework would be quite exciting.

This is an issue we did indeed consider when setting up the inversion. However, we do not think that the inclusion of a bias term in the GOSAT data is necessary in this work. The Turner et al (2015) paper highlights this latitudinal bias but shows that the bias is most pronounced at high latitudes and "becomes significant at latitudes polewards of 50". A similar point is made in Maasakkers et al (2019). Since our study area covers between 26S – 26N the bias is anticipated to be small (less than 5 ppb) and impacts of such a bias on derived emissions may not be as great as at higher latitudes.

Furthermore, a bias in background concentrations may be absorbed into the boundary condition terms in the regional inversion, since scale factors applied to these background fields were allowed to vary and solved for in the inversion. This is unlike a global inversion where we agree

any latitudinally dependent errors in model transport would make this bias correction term important.

Nevertheless, to address this reviewer's comment we have tested our prior assumptions about the importance of this bias at low latitudes by reporting further calculations. We have done so by applying the quadratic regression bias correction, $y = 0.005 * (x^2 – x – 100)$, from Turner et al. (2015) to the data (where y is the bias and x the latitude in degrees) and rerunning the PR1 inversion. This implies a bias of around 3 ppb at the N and S boundaries of our domain, tending to –0.5 ppb at the equator.

Total African emissions using PR1 data with the Turner bias correction applied are 72 (70-74) Tg yr^{-1} with a trend of 2.0 (1.6-2.4) Tg yr^{-1}. For comparison, without the bias correction emissions are 76 (74-78) Tg yr^{-1} for the PR1 inversion with a trend of 2.1(1.7-2.5) Tg yr^{-1}. The East Africa trend with the bias correction is 1.7 (1.4-2.0) Tg yr^{-1}, and without is 1.7 (1.4-2.0) Tg yr^{-1}. The Sudd emissions trend with the bias correction is 0.3 Tg yr^{-1}, with emissions increasing from 2.9 Tg yr^{-1} in 2010-2011 to 5.7 Tg yr^{-1} in 2015-2016, and without the bias correction emissions are 0.4 Tg yr^{-1}, with emissions increasing from 3.1 Tg yr^{-1} in 2010-2011 to 6.0 Tg yr^{-1} in 2015-2016.

We also reran the PR1 inversion using the bias correction term from Maasakkers et al (2019) which is very similar to that of Turner et al (2015) of the form: $y = 0.001 * (4x^2 – 1.3x) – 5$. The results from this test were almost identical to results from applying the Turner et al. (2015) bias correction, despite a different minimum (-5 vs –0.5). However, this absolute offset to all mole fractions can be absorbed in the boundary condition scaling, which we include as part of our state vector, and the shape of the latitudinal dependence between the two bias corrections is otherwise very similar.

The inclusion of a bias term has an impact on the total African emissions, reducing them by 4 Tg yr^{-1}, likely due to boundary condition scale factors needing to be slightly larger to account for the higher observed background mole fractions. However, the difference in the derived trends for Africa, East Africa and the Sudd are small and the main conclusions we draw in this work are unaffected. We propose this is for a number of reasons:

A) The region of interest is concentrated in the tropics where the change in bias term applied in Turner et al (2015) and Maasakkers et al (2019) was relatively small (less than 3 ppb).

B) We have 6 scaling terms for the boundary conditions. (N, NE, SE, S, SW and NW). As such, a latitudinal bias in air incoming to the domain could be accounted for by adjustments to these boundary conditions in the inversion.

C) The bias term is thought to be a stratospheric transport bias in the GEOS-Chem model, which is particularly evident at 4x5 degree resolution. Stanevich (2018) showed that the difference between GOSAT and GEOS-Chem is greatly reduced when a global simulation is performed at 2x2.5 degrees, and Maasakkers et al (2019) showed this difference is mostly in the simulation of

the stratosphere. Assuming that the bias magnitude is dependent on the model resolution, it could be further reduced at 0.5 x 0.625 used in the regional modelling of this work.

Since the bias may be resolution dependent, the 4x5 bias diagnosed by Turner et al (2015) and Maasakkers et al (2019) may not be appropriate for the higher resolution used here. Furthermore, since the identification of such a bias at 0.5x0.625 would be heavily dependent on the accuracy of emissions within the domain, we do not think it appropriate to apply an ad-hoc bias correction term to the GOSAT data in this work.

Solving for a latitudinally dependent bias term might be possible within the hierarchical approach, although it is not clear to us whether this may just act to counteract changes to the boundary condition scaling, such that neither parameter would obtain convergence within the MCMC framework.

In response to this comment we have included the results of the bias correction test in a new section at the end of the results to demonstrate that our assumption of no bias correction is not the driver of the results we find (section 3.4, P.15). We have also added some text to the methods to justify not including a bias correction in our main approach (section 2.2, P.6).

2.2 CO2 fields for the proxy method

It would be illustrative to also show a comparison between PR1, PR2, and a third case where the proxy retrievals are constructed using the full-physics XCO2 retrieval:

XCH4 proxy =XCH4 no−scatter/XCO2 no−scatter×XCO2 full−physics

This could be included in Figure 2, I don't think it's necessary for the authors to perform an additional inversion with this retrieval. It would, however, be nice to show a retrieval that is independent of modeled CO2 fields.

Whilst we understand the reviewer's viewpoint and agree it would be nice to have a proxy product independent of model CO2, in reality this isn't really directly comparable to the proxy products we use. The advantage of the proxy XCH4 product is that the spatial coverage is much greater than the full physics product due to the need to be less strict on the filtering of the data due to clouds and aerosols in the atmosphere. This is the reason for choosing to use the proxy XCH4 data as opposed to the full physics XCH4 retrieval, where the data coverage over tropical Africa is sparse. The retrieval of XCO2 is obviously beset by the same issues. As such a proxy XCH4 product based on a full physics XCO2 retrieval would lose the key coverage benefit of the proxy product and would not be directly comparable to the PR1 and PR2 data used in this work.

For the same reason we have chosen not to use a full physics XCH4 data product in this work as our initial tests showed there are not sufficient data within the full-physics product to constrain the CH4 fluxes on the scales that we do in the paper using the proxy XCH4 product. As such, the inversion result using full-physics retrievals do not differ markedly from the prior for large parts

of the domain, which is the subject of a manuscript in progress that studies pan-tropical changes in CH4 emissions using GOSAT data.

2.3 Number of MCMC samples

Page 7, Line 10 mentions that the a posteriori distributions each have 2,000 samples. However, aren't there 3,697 basis functions? Does that mean there are less than one sample per basis function? Do these posterior distributions really sample the full space?

There are 2000 samples that are retained to form the posterior distribution of each parameter (I.e. each a posteriori parameter distribution has 2000 individual values that approximate its PDF). The 2000 values that are stored are a sub-set of the 20,000 iterations that are run in the inversion (the Markov chain is thinned so only every 10^{th} iteration is stored). Each of the 3697 state vector elements are updated at each iteration. This has the joint effect of reducing storage space (2000 instead of 20,000 posteriori samples) and reducing correlation between stored samples if a proposal undergoes a number of consecutive rejections.

We have clarified this in the text with the following statement:

"Updates were proposed to each element of x every second iteration. At iterations in between, updates were proposed to all the theta values."

2.4 Mention 2010 LST anomaly discussion in the abstract

I think it's important that the authors mention that 2010 may be an anomalously low year for wetland emissions in the Sudd (based on their LST analysis). This paper will likely get quite a bit of attention because a number of groups are looking for trends in wetland emissions. The authors do an excellent job of discussing the nuances of their trends in the main text and conclusions, but I think there should be a short (less than one sentence) mention of this possible anomaly in 2010.

We agree that it is important to mention the caveats in the trend in emissions we have found and have included the following text in the abstract so that this is highlighted up front:

"Using satellite land surface temperature anomalies and altimetry data we find this increase in CH4 emissions is consistent with an increase in wetland extent due to increased inflow from the White Nile, although the data indicate that the Sudd was anomalously dry at the start of our inversion period."

2.5 Wolfe et al.

The authors should mention Wolfe et al., PNAS (2018): "Mapping hydroxyl variability throughout the global remote troposphere via synthesis of airborne and satellite

formaldehyde observations" and consider using this data to help constrain their OH fields in the future (would be beyond the scope here).

We thank the reviewer for bringing the Wolfe et al. (2018) study to our attention. Ultimately it would be insightful to incorporate multiple complementary datasets into an inversion framework in order to constrain separate production and loss processes. We have expanded the discussion section to make this point although, as the reviewer says, it is clearly beyond the scope of this work. We have added the following lines to the text:

"Incorporating additional information from complementary measurement data into the inversion system could further help to reduce uncertainties in the CH4 budget. Examples of potentially useful space-based measurements include formaldehyde to constrain the temporal and spatial variability of the OH radical sink (Wolfe et al. 2018). and GRACE data to help constrain the temporal variability of wetland emissions."

3 Specific comments:

Page 2, Line 23: Suggest replacing mathematically with mechanistically.

Agreed and replaced.

Page 3, Line 11: Suggest replacing strong signatures with a synonymous phrase. I typically associate "signatures" with isotopic source signatures, which are also discussed in the manuscript.

To avoid confusion we have replaced this line with the following text:

"…emissions from seasonal fires …"

Page 5, Lines 8–12: This paragraph seems out of place, I feel like it should go before the discussion of CO2 fields. Right now it goes –

>GOSAT details –>proxy retrievals–>CO2fields –>impact of CO2 fields –>back to GOSAT details.

To ensure a better flow we have moved this paragraph earlier as suggested.

Page 5, Line 31: I think you should move the Feng et al. (2017) citation to the beginning of Line 30. It initially sounded like you were building some Kriged global concentration fields

from the NOAA data because of this text ". . . coarser global run that was fitted to in situ data. . . "

Agreed, we have moved the citation.

Page 6, Line 4: Suggest replacing "prior" with " a priori" for consistency with the rest of the text.

We have changed the text as suggested to ensure consistency.

Reviewer 2

General comments

Lunt et al. constrain methane emissions in tropical Africa with GOSAT XCH data to retrieve monthly CH4 emissions in the framework of a Bayesian inversion. A very useful sensitivity test (to the CO2 fields used in the XCH) is included, which makes it possible to provide uncertainty ranges for the estimates of emissions and comment on the significance of the results. With satellite XCH4 data from 2010 to 2016, they are able to study seasonal cycles as well as the 7-year trend. Using various other satellite data (land surface temperature anomaly, altimetry), they are able to suggest links between their findings regarding CH4 emissions and the sources contributing to the variations of these emissions, which are mainly wetlands in this area. This study provides estimates for CH4 emissions and their variations at various spatial and temporal scales in an area, tropical Africa, which is both a key-region for methane emissions and a region where these emissions are very uncertain. The authors have been able to exploit not only satellite data of XCH4 to assimilate in their inversion framework, which already provides rich insights regarding methane emissions, but also to proceed further in the investigation of the possible drivers of the variations of these emissions, making use of different satellite data sets. The manuscript is clearly written and well-structured, the results are very clearly presented and discussed. For all these reasons, I recommend publication of this manuscript in ACP after minor corrections (most corrections for Section 2.3).

We thank Reviewer 2 for their assessment of the work and address their specific comments below.

Specific comments

p.2 l.31: what about wild animals for enteric fermentation?

Based on available literature (e.g. Crutzen et al 1986) we assume wild animals in Africa to mean gazelles and wildebeest. Crutzen et al (1986) estimated 1-5 Tg yr^{-1} for wild ruminants across all tropical regions. Perez-Barberia (2017) estimate 1.1-2.7 Tg yr^{-1} for all wild ruminants globally. As such the source is likely to be small when compared to agriculture and wetlands, and of a size comparable perhaps to termite methane production, although uncertainties on both these source types are large.

We have rephrased this sentence to say:

“The African continent contains significant microbial methane sources from wetlands and agricultural enteric fermentation, as well as smaller microbial sources from termites and wild ruminants (Crutzen, 1986; Sanderson, 1996).”

p. 2 l.33: indicate what the range corresponds to (one-sigma, 95%, the full range of the ensemble) so that the reader can compare to the other ranges in the paper.

We thank the reviewer for pointing out the lack of a definition for this range. The range represents the 5^{th} - 95^{th} percentile of the ensemble as defined in Bloom et al (2017). We have added this information to the text.

p.4 l.4: explanation for the year 2016?

We can only speculate on the cause of the difference but the timing of 2010 and 2015-2016 suggests El Nino related differences. A recent study has indicated a larger tropical African carbon source using satellite data than is estimated from in situ data (Palmer 2019). This difference would seem to explain the difference between proxy CH4 fields generated from in situ and satellite derived CO2 fields.

In response to this comment we have added the following text:

“The larger PR2 XCH4 levels in 2016 are a result of a larger net CO2 source being inferred from tropical Africa when using satellite data as opposed to *in situ* data (Palmer et al 2019).”

p.4 l.20: "as opposed to XCO2": I don’t understand the idea implied here.

We acknowledge that this phrase causes some unnecessary confusion and can be dispensed with. We have rephrased this sentence to say:

“In using the ratio to determine XCH4, we assume that atmospheric CO2 varies much less than CH4.”

p.6, Section 2.3: I think this Section is a bit confusing as it seems to be trying to explain a methodology but not in details so that some useful elements are missing for the reader and others are presented in too general a way. Some particular remarks below. Could you try re-writing the Section with a kind of clear hierarchy in the important points for understanding the study described in the paper and the general points which are detailed in the references?

We thank the reviewer for highlighting the confusing nature of this section and have followed the reviewer's suggestion in attempting to rewrite it in a way that is easier to follow.

Our intention was to provide a brief summary of the method that is described in much greater detail in Ganesan et al (2014) and Lunt et al (2016). However, from the reviewer's comments we see that this may have led to the feeling that we were trying to explain the method in this work, albeit inadequately. To avoid this situation, we have referred the reader to the references for the details of the inversion approach and its benefits. In this rewritten section we attempt to make clear we are briefly summarizing the method by means of introduction before focusing on the specifics of this work, and how the hierarchical approach is set-up.

We have restructured this section to follow the structure below:

A) Brief overview of the general hierarchical Bayesian format

B) Description of the a priori state vector in this work

C) Description of the a priori parameters vector.

D) Description of the sensitivity matrix formulation

E) Description of the MCMC setup.

We hope that this is easier to follow as a result.

Please see the marked up new version of the text and the response to specific comments below for further changes.

> *p.6 l.28: "reducing the impact of underlying assumptions": I think it is a bit optimistic to put it like this. The assumptions are still there but they are not made on the same variables/parameters. For instance, the assumption that the errors can be specified as PDFs and, then, the user's choice of one given type and form (be it Gaussian, Poisson or another).*

We agree that investigator assumptions must always be made somewhere and perhaps it might be better phrased as saying the assumptions are one extra step removed from the posterior distribution. I.e. The assumptions are made on the hyper-parameters (i.e. the uncertainty in the uncertainty) and not on the uncertainty parameters themselves. Given the restructuring that we have done to this section in response to the previous point, this line no longer appears in the text.

> *p.6 l.30: "uncertainties in the a posteriori distribution are more representative of uncertainties in the inversion system": more representative than what?*

We thank the reviewer for highlighting the phrasing of this sentence and we have rewritten it to say:

"Equation 3 indicates that uncertainties in theta propagate through to the a posteriori distribution of x, which is one of the benefits of this approach given the a priori and model uncertainties may not be well known."

p.6 l.31: "any form of error variances can be used": do you mean covariances? "Any form" is misleading: they still need to be PDFs, probably ones defined by only a few parameters.

Indeed, we were attempting to make the point that there is flexibility in the form of PDF that is chosen, and used "any form" within the context of PDFs. We have rephrased this to say:

"In addition, the choice of a priori or measurement PDF is open to the investigator, which allows flexibility in cases where, for example, the PDF should be defined only on the positive axis."

p.7 l.12: "all parameters in turn": does it mean one parameter per iteration?

For the avoidance of doubt, we meant that all state vector elements are updated at each iteration. We have rewritten this line to make this point clearer. The line now reads:

"Updates were proposed to all elements of x every second iteration. At iterations in between, updates were proposed to all theta values."

p.7 l.13: which are the hyper parameters here?

We realise we have erroneously referred to parameter updates as hyper-parameter updates. To be clearer we define x as the state vector, σ_x and σ_y as the parameters and the uncertainty in σ_y as the hyper-parameters. We have corrected any incorrect specification throughout the text.

p.7 l.27: what is the type and form of the posterior distribution?

The posterior distribution is undefined, since it is formed from some combination of Gaussian (likelihood function) and log-normal (prior distribution) distributions, hence the need for a MCMC approach to approximate its form.

In reality, as the violin plots in the new Figure 4 show (see response to p8. L17, fig 3 further down), the form is not too dissimilar from Gaussian.

p.7 l.20: reference for the measurement uncertainty? Same in both XCH4?

GOSAT retrieval uncertainties are from the dataset of Parker (2015) and are the same for both PR1 and PR2. We have added this information to the text.

p.7 l.23: can you comment a bit on the validity of the "uncorrelated" assumption?

The primary governor of this decision to assume diagonal observation error matrices was the computational cost, however we accept that this assumption of uncorrelated errors is likely to lead to an underestimate of the posterior uncertainties compared to the case where error correlations are included, since too much weight may be given to individual observations.

Correlated measurement uncertainties can, in effect, reduce the number of independent measurements. However, the decision about the scales over which this correlation should apply are difficult to quantify and usually subjective. Chevalier (2007) showed that using error inflation could partly compensate for neglecting the contribution of error correlations, and avoid over-constraining the a posteriori emissions. In our inversions we include both a measurement uncertainty, which is part of the data product from Parker et al (2015), and a second term that is allowed to vary within the inversion and partly acts to inflate the error. We set a minimum value of 5 ppb for this term and constrain it within the inversion. The a posteriori mean value across all timesteps for this additional model uncertainty term is 8 ppb, of a similar magnitude to the 9 ppb mean measurement uncertainty, and leads to an increase in the error term. We note that Turner et al (2015) suggested that the uncertainties of Parker et al (2015) were already a conservative estimate of uncertainty. In addition the mean minimum distance between GOSAT retrievals from the UoL proxy dataset is around 225 km, a distance over which it has been suggested in regional CH4 inversion studies measurements may be largely uncorrelated (Ganesan et al, 2017).

In response to this comment we have expanded on the validity of this assumption in the text as follows:

“Due to the density of data, and to make the inversions more computationally tractable we assumed measurement errors were spatially and temporally uncorrelated. Although this might result in an underestimate of the posterior uncertainties, one approach to form a diagonal approximation of a full covariance matrix is through error inflation (Chevalier 2007). The inclusion of a model uncertainty term in our inversions, in addition to the measurement uncertainty, partly acts to inflate the error. This additional error term is allowed to vary in the inversion, and constrained by the data, but is of a similar magnitude to the measurement uncertainty, with a mean a posteriori value of 8 ppb, leading to an increase in the error term. In addition, Turner et al (2015) suggested that the measurement uncertainties of Parker et al (2011) were already a conservative estimate of uncertainty, further adding to the observation error inflation.”

p.8 l.11: you should also report the range for the Saunois et al. figure, so that the following conclusion (l. 15-16) that your results are consistent with it is actually supported. You can also make use of Saunois et al. 2017: https://doi.org/10.5194/acp-17-11135-2017

Agreed. We have added the range of the Saunois estimates in addition to the mean value that was originally included.

p.8, l.17: Fig 3: it is difficult to interpret the fact that the prior is outside the posterior 95% uncertainty range without any information on the types and forms of the PDFs. Maybe something like Fig 4 of http://dx.doi.org/10.1016/j.spasta.2016.06.005 could be useful?

We agree that something like the suggested plot would be nice to show as it conveys a lot of information in a single plot. However, it is difficult to apply it in this case, due to the irregular nature of the state vector making it hard to plot the violin plots on a regular grid in a manner that would also convey the geographical location of each of the state elements. We could plot the data as a standalone violin plot but we are conscious of the fact that a reader's geography may need to be guided by a map.

Therefore, we have kept the existing panel c) but added an additional figure containing a violin plot for each of the African regions of the state vector. The regions run from South to North up the y-axis, with the violins showing the a posteriori distributions in Tg yr^{-1}, for both the PR1 and PR2 inversions. Red crosses show the a priori mean for each region. We hope it is clear to see from this plot the areas where both posteriors are much greater than the prior mean (e.g. Sudd, Ethiopia, Mozambique, Chad) and those that are much less (Cuvette Centrale and N. DRC).

We have added some additional text that refers to this figure and highlights the regions where the a posteriori distribution is much larger or smaller than the a priori mean.

"This is further highlighted in Fig. 4, which shows the multi-year average a posteriori distributions from both PR1 and PR2 inversions and the a priori mean for each of the basis function regions. The a priori mean value lies outside the 95 percentile range for many of the distributions over the East African regions."

p.9, Section 3.1: make use of Saunois et al. 2017: they discuss the variability over 2000-2012 so that there are only three years common with your period but you could put your trends in perspective.

We have added some additional text which makes reference to Saunois et al (2017) in the discussion section (Section 4), where we attempt to put our work in the context of other studies.

p.9 l.13: "although there was substantial inter-annual variability": I don't understand the logical link between the inter-annual variability (which can go either way from one year to the other) and the trend.

Indeed, we did not intend to intimate a link between inter-annual variability and the trend. We meant that the inter-annual variability might mask any underlying trends over the inversion period.

We have rephrased this statement to say:

"We found no other consistent trends regional trends between the PR1 and PR2 inversions over the inversion period, although there was substantial inter-annual variability which might mask any underlying trends, particularly over West Africa…"

p.9 l.22: why are the glint data more sensitive to the boundary conditions?

The glint data may be more sensitive to the boundaries by virtue of being closer to the boundaries of the domain, and thus any changes to the boundary scaling has a greater impact on the fit to the data. We have added this statement to the text:

"(which are more sensitive to the scale factors applied to the domain boundaries due to their proximity to the edge of the domain)"

p.11 l. 4-6: indicate whether the link between the variations of LST anomalies and wetland extent variations is a (reasonable) assumption or a proven proxy link. Maybe with a reference?

LST anomaly data has been used extensively in the meteorological literature as a proxy for soil moisture. When the soil is wet more energy will go to latent heat flux as opposed to sensible heat flux leading to a decrease in the LST. For example, Taylor (2015) compared LST anomalies to independent soil moisture anomalies from the advanced scatterometer (ASCAT) instrument to confirm that LST anomalies are related to soil moisture anomalies through the surface energy balance response. Cammalleri and Vogt (2015) showed that LST can be used directly as a proxy of soil moisture with the best results over areas characterized by water-limited conditions. In response to this comment we have edited these lines to attempt to make this point more explicitly:

"The use of satellite LST data as a proxy for soil moisture is well-established (e.g. Cammalleri and Vogt 2015, Folwell 2016, Gallego-Elvira 2016). In dry conditions, evaporation of water from the soil is restricted, the ratio of latent heat to sensible heat flux decreases and thus the surface temperature increases (Byrne, 1979; Cammalleri and Vogt, 2015). As such, areas of elevated soil

moisture exhibit cooler surface temperatures than dry soil and hence lower LST. The LST anomaly from the climatological monthly mean LST …"

p.13 l.4: "r2 values of 0.2-0.8": 0.2 does not seem to be such a strong correlation. Do you have criteria for the significance of this?

We thank the reviewer for highlighting this, and we have expanded on the correlation coefficients and added them to each of the individual panels of Fig. 7 to be clearer about which regions show a reasonable correlation between emissions and LWE anomalies. The 0.2 figure is from the Angola/Zambia region which has a significant biomass burning component to emissions which would appear to lessen the correlation to LWE anomaly. The largest correlation coefficients should be 0.7 (not 0.8 as was written in error) for the Chad, Sudan, South Sudan, Madagascar and Niger Basin regions. Some of the regions exhibit a smaller secondary emissions peak that reduces the correlation with LWE anomaly, but the correlation between LWE anomaly and the major seasonal CH4 emissions peak remains dominant. The text now reads:

"Chad, Sudan, South Sudan, Madagascar and the Niger Basin in particular show the strongest correlations with r^2 values of 0.7 as shown in Fig. 8."

p.15. l.1 seq: make use of Saunois et al. 2017.

We attempted to use references that covered global emissions over a period similar to the one in this work. However, we are happy to also make use of the Saunois reference if it helps to put the results in context. We have added the following lines to the text:

"Although Saunois et al (2017) found emissions from the tropics to have increased by 18 (13-24) Tg yr^{-1} between the periods 2002-2006 and 2008-2012, relatively little of this was ascribed to Africa. This is qualitatively consistent with our hypothesis that the increase in emissions from East African regions due to increased water levels of the East African lakes was limited to the period between 2010 and 2016."

Technical corrections

fig 1 (a): what is the background of the map: climatological vegetation cover?

The background is a shaded relief map from natural earth https://www.naturalearthdata.com. We have added this information to the figure caption.

p.3 l.19: "Gravity Recovery and Climate Experiment (GRACE,"->And

Corrected.

p.3 l.20: "liquid water equivalent height (LWE) height anomaly retrievals" -> delete first height

Corrected.

p.4 l.31: "different to" -> different from?

Corrected.

p.7 l.28: "clearly show" -> clearly shows

Corrected

p.8 l.17 seq.: there are a lot of numbers in the two paragraphs: would it be possible to make a table? E.g. with columns prior, PR1 posterior, PR2 posterior. Same remark for p.9 l.2 seq., p. 10 first paragraph

Whilst we appreciate it may not be to everyone's liking, we have included several numbers in the text as we feel this it is important to quantify our results. We have also endeavoured where possible to present these graphically through the figures. We hope the inclusion of the additional violin plot (Figure 4) has helped to convey the results more clearly and feel that this minimizes the need for any additional tables.

p.8 l.33: "that" -> than (smaller l. 32)

Corrected.

p.9 l.12: "reigon" -> region

Corrected.

p.10 l.18: "represents" -> represent

Corrected.

p.11 l.4: "anomalies from" -> "anomalies of"?

Corrected.

p.11 l.30: missing)

Corrected.

p. 15 l.32: "changes" -> change

Corrected.

References:

Byrne, G. F., Begg, J. E., Fleming, P. M., and Dunin, F. X.: Remotely sensed land cover temperature and soil water status—a brief review, Remote Sensing of Environment, 8, 291–305, https://doi.org/10.1016/0034-4257(79)90029-4, 1979.

Cammalleri, C. and Vogt, J.: On the Role of Land Surface Temperature as Proxy of Soil Moisture Status for Drought Monitoring in Europe,Remote Sensing, 7, 16 849–16 864, https://doi.org/10.3390/rs71215857, 2015.

Chevallier, F.: Impact of correlated observation errors on inverted CO2 surface fluxes from OCO measurements, Geophysical Research Letters, 34, https://doi.org/10.1029/2007gl030463, 2007.

Crutzen, P. J., Aselmann, I., and Seiler W: Methane production by domestic animals, wild ruminants, other herbivorous fauna, and 30 humans, Tellus B, 38B, 271–284, https://doi.org/10.1111/j.1600-0889.1986.tb00193.x, 1986.

Maasakkers, J. D., Jacob, D. J., Sulprizio, M. P., Scarpelli, T. R., Nesser, H., Sheng, J.-X., Zhang, Y., Hersher, M., Bloom, A. A., Bowman, K. W., Worden, J. R., Janssens-Maenhout, G., and Parker, R. J.: Global distribution of methane emissions, emission trends, and OH concentrations and trends inferred from an inversion of GOSAT satellite data for 2010–2015, Atmospheric Chemistry and Physics, 19, 7859–7881, https://doi.org/10.5194/acp-19-7859-2019, 2019.

Palmer, P. I., Feng, L., Baker, D., Chevallier, F., Bösch, H., and Somkuti, P.: Net carbon emissions from African biosphere dominate pantropical atmospheric CO2 signal, Nature Communications, 10, https://doi.org/10.1038/s41467-019-11097-w, 2019

Parker, R. J., Boesch, H., Byckling, K., Webb, A. J., Palmer, P. I., Feng, L., Bergamaschi, P., Chevallier, F., Notholt, J., Deutscher, N., Warneke, T., Hase, F., Sussmann, R., Kawakami, S., Kivi, R., Griffith, D. W. T., and Velazco, V.: Assessing 5 years of GOSAT Proxy XCH4 data and associated uncertainties, Atmospheric Measurement Techniques, 8, 4785–4801, https://doi.org/10.5194/amt-8-4785-2015, 2015.

Taylor, C. M. (2015), Detecting soil moisture impacts on convective initiation in Europe. Geophys. Res. Lett., 42, 4631– 4638. doi: 10.1002/2015GL064030.

Turner, A. J., Jacob, D. J., Wecht, K. J., Maasakkers, J. D., Lundgren, E., Andrews, A. E., Biraud, S. C., Boesch, H., Bowman, K. W., Deutscher, N. M., Dubey, M. K., Griffith, D. W. T., Hase, F., Kuze, A., Notholt, J., Ohyama, H., Parker, R., Payne, V. H., Sussmann, R., Sweeney, C., Velazco, V. A., Warneke, T., Wennberg, P. O., and Wunch, D.: Estimating global and North American methane emissions with high spatial resolution using GOSAT satellite data, Atmospheric Chemistry and Physics, 15, 7049–7069, https://doi.org/10.5194/acp-15-7049-2015, 2015

An increase in methane emissions from tropical Africa between 2010 and 2016 inferred from satellite data

Mark F. Lunt[1], Paul I. Palmer[1,2], Liang Feng[1,2], Christopher M. Taylor[3,4], Hartmut Boesch[5,6], and Robert J. Parker[5,6]

[1]School of GeoSciences, University of Edinburgh, Edinburgh, UK
[2]National Centre for Earth Observation, University of Edinburgh, Edinburgh, UK
[3]Centre for Ecology and Hydrology, Wallingford, UK
[4]National Centre for Earth Observation, Wallingford, UK
[5]Earth Observation Science, Department of Physics and Astronomy, University of Leicester, Leicester, UK
[6]National Centre for Earth Observation, University of Leicester, Leicester, UK

Correspondence: Mark Lunt (mark.lunt@ed.ac.uk)

Abstract.

Emissions of methane (CH_4) from tropical ecosystems, and how they respond to changes in climate, represent one of the biggest uncertainties associated with the global CH_4 budget. Historically, this has been due to the dearth of pan-tropical *in situ* measurements, which is particularly acute in Africa. By virtue of their superior spatial coverage, satellite observations of atmospheric CH_4 columns can help to narrow down some of the uncertainties in the tropical CH_4 emission budget. We use proxy column retrievals of atmospheric CH_4 (XCH_4) from the Japanese Greenhouse gases Observing SATellite (GOSAT) and the nested version of the GEOS-Chem atmospheric chemistry and transport model ($0.5° \times 0.625°$) to infer emissions from tropical Africa between 2010 and 2016. Proxy retrievals of XCH_4 are less sensitive to scattering due to clouds and aerosol than full physics retrievals but the method assumes that the global distribution of carbon dioxide (CO_2) is known. We explore the sensitivity of inferred *a posteriori* emissions to this source of systematic error by using two different XCH_4 data products that are determined using different model CO_2 fields. We infer monthly emissions from GOSAT XCH_4 data using a hierarchical Bayesian framework, allowing us to report seasonal cycles and trends in annual mean values. We find mean tropical African emissions between 2010–2016 range from ~~75 (72~~76 (74–78) Tg yr^{-1} to 80 (78–~~83~~82) Tg yr^{-1}, dependent on the proxy XCH_4 data used, with larger differences in northern hemisphere Africa than southern hemisphere Africa. We find a robust positive linear trend in tropical African CH_4 emissions for our seven-year study period, with values of 1.5 (1.1–1.9) Tg yr^{-1} or 2.1 (1.7–2.5) Tg yr^{-1}, dependent on the CO_2 data product used in the proxy retrieval. This linear emissions trend accounts for around a third of the global emissions growth rate during this period. A substantial portion of this increase is due to a short-term increase in emissions of 3 Tg yr^{-1} between 2011 and 2015 from the Sudd in South Sudan. Using satellite land surface temperature anomalies and altimetry data we find this increase in CH_4 ~~emission~~ emissions is consistent with an increase in wetland extent due to increased inflow from the White Nile, although the data indicate that the Sudd was anomalously dry at the start of our inversion period. We find a strong seasonality in emissions across northern hemisphere Africa, with the timing of the seasonal emissions peak coincident with the seasonal peak in ground water storage. In contrast, we find that *a posteriori*

CH_4 emissions from the wetland area of the Congo basin are approximately constant throughout the year, consistent with less temporal variability in wetland extent, and significantly smaller than *a priori* estimates.

1 Introduction

The recent and ongoing rise in atmospheric CH_4 since 2007, after a period of relative stability, has been well documented, although the causes are still not fully understood (e.g. Rigby et al., 2008; Nisbet et al., 2014; Turner et al., 2019). Dominant sources of CH_4 to the atmosphere are both natural and anthropogenic including fossil fuels, agriculture, waste management and natural wetlands (Kirschke et al., 2013; Saunois et al., 2016), whilst the major sink is due to reaction with the hydroxyl radical (OH) in the troposphere. Several hypotheses have been suggested that could explain recent changes in atmospheric CH_4 but none are verifiable because of a lack of data at the global scale (Turner et al., 2019). These hypotheses include increased fossil fuel emissions, increased microbial emissions, or some combination of the two allied with other factors (e.g. Schaefer et al., 2016; Hausmann et al., 2016; Worden et al., 2017; McNorton et al., 2018; Thompson et al., 2018). Additionally, we cannot discount a role for a changing OH sink based on CH_4, isotopic $\delta^{13}CH_4$ and methyl chloroform observations (Rigby et al., 2017; Turner et al., 2017).

One of the plausible explanations is that tropical microbial emissions have increased (Nisbet et al., 2016; Schaefer et al., 2016; Thompson et al., 2018). This hypothesis is based largely on a significant negative trend in $\delta^{13}CH_4$ isotope values globally and the latitudinal distribution of CH_4 growth rates. Microbial sources are more depleted in $\delta^{13}CH_4$ than other sources so that a move to lighter isotope values can be interpreted as microbial sources providing a greater proportion of total CH_4 emissions. However, $\delta^{13}CH_4$ source signatures for different microbial sources and their variation over time are not well characterized (Turner et al., 2019). As a result the constraint provided by isotope data is limited to broad-scale inferences on changes in sources and sinks, and cannot narrow down which type of microbial source is responsible. Additional independent information, such as that from process-based based wetland models, can provide further evidence for changes in microbial sources. For example, some individual wetland model studies suggest that wetland CH_4 emissions have increased (e.g. McNorton et al., 2016; Zhang et al., 2018), although the increases are relatively small and likely to be model dependent (Poulter et al., 2017).

One of the main challenges associated with studying wetland emissions of CH_4 is that they are difficult to describe ~~mathematically~~mechar
Process-based wetland models use parameterizations of biological processes informed by field data, together with estimates of the spatial extent of wetland, to describe the seasonal magnitude and distribution of wetland emissions across the globe. The extent of wetland area is usually prescribed from climatology (Lehner and Doll, 2004; Bergamaschi et al., 2007), determined from a hydrological model (Gedney and Cox, 2003) or parameterized using remotely sensed inundation datasets (Prigent et al., 2007; Schroeder et al., 2015). Because the spatiotemporal variability of wetland extent is key to estimating CH_4 emissions, disagreement between different measures of wetland areas equates to a wide range of emission estimates (Melton et al., 2013).

The African continent contains significant microbial methane sources from wetlands ~~as well as~~ and agricultural enteric fermentation, as well as smaller microbial sources from termites and wild ruminants (Crutzen et al., 1986; Sanderson, 1996) . A recent study, comprising an ensemble of wetland emissions models, estimates African wetland CH_4 emissions represent 12 (7–23)% of global wetland emissions (Bloom et al., 2017), where the numbers in parentheses indicate the 95 percentile range. These emissions are concentrated in the sub-Saharan tropics, where we focus our work. Figure 1(a) shows our study domain that includes all the main wetland regions within Africa, including the Congo Basin located in Central Africa and the Sudd in South Sudan. For the purposes of our study we use a very broad definition of wetlands to include any areas of land that are permanently or periodically inundated.

Due to the seasonal migration of the Intertropical Convergence Zone (ITCZ), rains fall in the sub-Saharan lands of northern hemisphere Africa during boreal summer, and in the southern hemisphere Africa during austral summer. Wetland extents vary with this delineation of wet and dry seasons, with maximum wetland extents generally occurring at the end of each rainy season (Taylor et al., 2018). The contribution from different wetlands to continental-scale CH_4 emissions is uncertain. Consequently, there is considerable disagreement between wetland emission models about the distribution and magnitude of CH_4 emissions, particularly regarding the timing of the seasonal peak of emissions between 0–15 °N, with models predicting peak ~~emission~~ emissions to occur in February, April–October or September–November (Bloom et al., 2017). The uncertainty in African CH_4 emissions is compounded by uncertainties associated with emissions from ~~fires which have strong signatures at certain times of the year~~ seasonal fires, and agricultural CH_4 emissions, ~~particularly~~ especially enteric fermentation from livestock. Enteric fermentation estimates are based on uncertain activity data and Tier 1 emissions factors from the Intergovernmental Panel on Climate Change (IPCC), with studies suggesting these emission factors are either too low (Kouazounde et al., 2014; Toit et al., 2014; Wolf et al., 2017) or too high (Goopy et al., 2018), and should be country dependent.

The tropics, particularly Africa, are generally poorly sampled by *in situ* atmospheric measurement networks. As such, this is where satellite data have the greatest potential to develop current understanding of CH_4 emissions, despite the requirements for cloud-free scenes. Bloom et al. (2010, 2012) used dry air column averaged methane mole fraction (XCH_4) data from the SCIAMACHY satellite (Frankenberg et al., 2011) and Gravity Recovery ~~and~~ And Climate Experiment (GRACE, (Tapley et al., 2004)) liquid water equivalent ~~height~~ (LWE) height anomaly retrievals to show that the seasonal cycle of wetland CH_4 emissions can largely be explained by seasonal changes in water volume in the tropics, and temperature in the high latitudes. More recently, Parker et al. (2018) compared peak-to-peak seasonal cycles of XCH_4 from models and the Greenhouse gases Observing SATellite (GOSAT) over tropical wetlands including those in Africa. They find significant discrepancies between model estimates, driven by a range of wetland emission estimates, but do not determine the magnitude of the CH_4 emissions that are consistent with the GOSAT data.

In this work, we infer CH_4 emissions over tropical Africa from 2010 to 2016 (Figure 1) from GOSAT XCH_4 data using the GEOS-Chem 3-D chemistry transport model, driven by *a priori* emission estimates, and a Bayesian inversion method. The data and methods we use are described in section 2. Previous studies of atmospheric CH_4 using satellite data tend to be global in scope with *a posteriori* emission estimates inferred over large continental regions (e.g. Fraser et al., 2013; Pandey et al., 2016; Feng et al., 2017), although some studies use satellite data in regional inversions to infer emissions on smaller regional scales

(Turner et al., 2015; Ganesan et al., 2017; Miller et al., 2019). Recent work using GOSAT XCH_4 data has suggested that both atmospheric CH_4 mole fractions and CH_4 emissions from the African continent have increased since 2009 (Maasakkers et al., 2019; Miller et al., 2019). Here, we take advantage of a nested capability of GEOS-Chem, allowing us to study atmospheric CH_4 with a spatial resolution of $0.5° \times 0.625°$, driven by coarser resolution lateral boundary conditions provided by the same model. We report our results in section 3, including regional seasonal and annual mean variations. We focus our attention on significant increased emissions from the Sudd wetlands and use correlative data to propose the underlying mechanism. We conclude the paper in section 4.

2 Data and Methods

2.1 GOSAT XCH_4 data

GOSAT was launched in 2009 into a sun-synchronous orbit with a local equator crossing time of 13:00, resulting in global coverage every three days (Kuze et al., 2009). We use data from the Thermal And Near infrared Sensor for carbon Observations - Fourier Transform Spectrometer (TANSO-FTS) that measures short wave infrared (SWIR) radiances between 0.76–2.0 μm at a resolution of 0.3 cm^{-1} from which dry air column averaged CH_4 values are retrieved (Parker et al., 2011). We use the University of Leicester's (UoL) v7 GOSAT-OCPR proxy XCH_4 product (Parker et al., 2015). These data have been previously validated against ground-based data from the Total Carbon Column Observing Network (TCCON, Wunch et al., 2011), with a global mean bias of +4.8 ppb and a single sounding precision of 13.4 ppb (Parker et al., 2015). The TCCON data available in the tropics agree reasonably well with these GOSAT data, with a positive bias of 3.1 ppb at Ascension Island and 3.4 ppb at Paramaribo, Suriname (Parker et al., 2018). However, there are currently no TCCON stations in tropical Africa.

We use GOSAT-OCPR proxy XCH_4 data over our study domain described by 20°W–55°E, 26°S–26°N. Retrievals are filtered for cloud-free scenes by retaining data where the surface pressure difference between the O_2-A band apparent surface pressure retrieval and the corresponding ECMWF surface pressure is within 30 hPa and where the signal-to-noise ratio is above 50 (Parker et al., 2015). We use both nadir and glint observations in this work, although we assess the impact of using only nadir observations to infer *a posteriori* CH_4 emissions in Section 3.1.

The proxy XCH_4 data is given by:

$$XCH_{4\ \mathrm{proxy}} = \frac{XCH_4}{XCO_2} \times XCO_{2\ \mathrm{model}}, \quad (1)$$

where XCH_4 and XCO_2 are the retrieved column values of the CH_4 and CO_2 respectively (Parker et al., 2015). These values are retrieved in neighbouring spectral windows at 1.65 μm and 1.61 μm for CH_4 and CO_2 respectively, meaning that common factors that impact the retrievals, e.g. aerosol and cloud scattering, can be removed by taking the ratio. The "proxy" column CH_4 is then determined by multiplying by an independent estimate of the XCO_2, typically from an atmospheric model. ~~By~~ In using the ratio to determine XCH_4, ~~as opposed to XCO_2,~~ we assume that atmospheric CO_2 varies much less than CH_4~~, and that it is sufficiently well known (e. g. from a model).~~. The main advantage of this data product is that it is more robust than the full physics approach in the presence of clouds and aerosols. This is particularly important over the tropics where clouds are

prevalent during the wet season and biomass burning aerosols are widespread during the dry season. However, this approach propagates model CO_2 errors to the proxy XCH_4 data product and subsequently to *a posteriori* emission estimates.

Here, we assess the sensitivity of our *a posteriori* CH_4 emission estimates to different model fields of CO_2. Our control XCH_4 data, PR1, is based on the standard UoL XCH_4 dataset, which uses the median XCO_2 field from three models (Parker et al., 2015). The second XCH_4 data product, PR2, uses $XCO_{2\ model}$ generated using a consistent version of the GEOS-Chem atmospheric chemistry transport model (described below) run at a spatial resolution of $4° \times 5°$ with emissions inferred using an ensemble Kalman filter (Feng et al., 2016) from the GOSAT ACOS XCO_2 data (O'Dell et al., 2012). Previous work has shown that CO_2 flux estimates from GOSAT for northern tropical Africa are larger than those inferred from *in situ* CO_2 mole fraction data (Houweling et al., 2015). Consequently, PR2 XCH_4 proxy data are significantly different ~~to~~ from PR1 XCH_4 data.

Figure 2 shows maps of the annual mean difference between the PR1 and PR2 XCH_4 data from 2010 to 2016. In general, the PR2 XCH_4 data are larger than the PR1 XCH_4, with a mean difference of 1.6 ppb over the seven-year period. The largest differences ($\simeq$ 10 ppb) are found over West Africa in 2010, over the Democratic Republic of Congo and Southern Africa in 2015 and over almost all of tropical Africa in 2016. In 2016, the mean of the PR2 XCH_4 data was 3.1 ppb larger than PR1. The larger PR2 XCH_4 levels in 2016 result from large net CO_2 emissions over tropical Africa inferred from satellite observations of XCO_2 (Palmer et al., 2019). With the exception of 2016, the smallest annual mean differences are generally observed over East Africa and north of 15°N. The spatial heterogeneity of the differences shown in Figure 2 illustrates the importance of assessing the sensitivity of the inversions to different XCH_4 proxy datasets, and we present inversion estimates based on both sets of data in our results.

~~We use GOSAT-OCPR proxy XCH_4 data over our study domain described by 20°W–55°E, 26°S–26°N. Retrievals are filtered for cloud-free scenes by retaining data where the surface pressure difference between the O_2-A band apparent surface pressure retrieval and the corresponding ECMWF surface pressure is within 30 hPa and where the signal-to-noise ratio is above 50 (Parker et al., 2015). We use both nadir and glint observations in this work, although we assess the impact of using only nadir observations to infer a posterioriCH_4 emissions in Section 3.1.~~

2.2 GEOS-Chem Atmospheric Chemistry Transport Model

We use a nested version of the GEOS-Chem atmospheric chemistry transport model (v11-01, Bey et al., 2001; Wecht et al., 2014; Turner et al., 2015) to relate surface emissions of CH_4 to atmospheric mole fractions. The model is driven by MERRA-2 reanalysis meteorological fields (Bosilovich et al., 2016), provided by the Global Modeling and Assimilation Office (GMAO) at NASA Goddard Space Flight Center. The native spatial resolution of these data is 0.5°(latitude)×0.625° (longitude), and includes 47 vertical terrain-following sigma-levels that describe the atmosphere from the surface to 0.01 hPa of which about 30 are typically below the dynamic tropopause. The 3-D meteorological data are updated hourly, and 2-D fields and surface fields are updated every 3 h. The atmospheric transport and chemistry time steps are five and ten minutes, respectively.

The nested region is focused on tropical Africa (Figure 1) described by 20°W–55°E, 26°S–26°N. Input emission fields to the nested GEOS-Chem run included wetlands (WetCHARTS, Bloom et al., 2017), biomass burning (GFED, v4, van der Werf et al., 2017), anthropogenic sources including agriculture, waste and energy (EDGAR, v4.3.2, Janssens-Maenhout et al.,

2017), and termites (Fung et al., 1991). Both WetCHARTs and GFED *a priori* emissions vary monthly between 2010–2016. EDGAR emissions from 2012 were used for all years for anthropogenic emissions. CH_4 loss due to oxidation by the hydroxyl radical (OH) in the troposphere is computed using a climatology of monthly OH concentration fields from a full-chemistry GEOS-Chem simulation, resulting in a lifetime with respect to tropospheric OH of 9.9 years (Wecht et al., 2014). Additional minor sinks of stratospheric oxidation (Murray et al., 2012) and a soil sink term (Fung et al., 1991) result in a global mean CH_4 atmospheric lifetime of 8.8 years.

At the boundaries of the nested domain we use time-dependent lateral boundary ~~conditions archived by a coarser global model run at $4° \times 5°$ that was fitted to in situdata from the National Oceanic and Atmospheric Administration (NOAA) network of sites. More comprehensive descriptions of this global~~ condition fields from a global optimization of CH_4 fluxes~~using in-situ data can be found~~ , described in Feng et al. (2017), the details of which we briefly summarise here. Global monthly methane emissions were optimized from spatial regions that were sub-divisions of the TransCom-3 regions using an ensemble Kalman filter approach from *in situ* CH_4 data. The global GEOS-Chem model at $4° \times 5°$ was used to relate fluxes to the observations from the National Oceanic and Atmospheric Administration (NOAA) network of sites. The resulting *a posteriori* fluxes were used to generate the global CH_4 fields for use in the lateral boundary conditions of the nested model, with the forward model initialised in January 2009 to minimize the influence of initial conditions. We stress that these global model boundary condition fields were ~~used as a prior~~ only used *a priori* in our nested model inversions, and updated in our inversion via *a posteriori* scaling factors based on the GOSAT data.

Previous work using GEOS-Chem in GOSAT XCH_4 inversion studies have included a latitudinally dependent bias term, which has been attributed to errors in the stratospheric transport of CH_4 within the GEOS-Chem model (Turner et al., 2015; Maasakkers et a . The form of this model bias is most pronounced at high latitudes and is particularly prevalent in the 4x5° model, and thus may be resolution dependent (Maasakkers et al., 2019). Given our region of study is in the tropics where the bias is small and we use a much higher resolution model we have not included a bias correction term in this work. However, we include some sensitivity tests to this potential model bias in Section 3.4.

2.3 Hierarchical Bayesian Inversion Method

To infer *a posteriori* CH_4 fluxes from the GOSAT XCH_4 data between January 2010 to December 2016 we ~~calculate the sensitivity of these data to emissions, boundary conditions, and the initial conditions. We calculate the monthly sensitivity of the data to emissions from a total of 38 regions across tropical Africa (Figure 1(b)). These regions are informed by national boundaries and major river basins or wetlands such as the Congo and Sudd. We include an additional six basis functions to describe monthly boundary condition scaling to the global CH_4 model field at the north, north-east, south-east, south, south-west and north-west boundaries. We also include a basis function to describe the initial 3-D CH_4 mole fraction distribution within the nested domain at the start of the inversion period. In total, we calculated 3697 basis functions over our seven-year study period.~~

~~To calculate the sensitivity of the XCH_4 data to emissions from each of our basis function regions (Figure 1(b)), we ran the forward model for one month, with emissions in each basis function based on the a prioridistribution. After one month the~~

emissions were turned off and we tracked 3-D CH_4 mole fraction field for a further three months as the signal decayed in the study domain due to atmospheric transport processes. After three months the residual signal due to perturbed emissions was negligible, so that we assumed zero sensitivity after this point. We sampled the model at the time and location of each GOSAT observed scene, and convolved the resulting model CH_4 profile with scene-dependent GOSAT averaging kernels to create the sensitivity matrix, $\mathbf{H}$. We compared the GOSAT XCH_4 values, use a hierarchical Bayesian inversion method. We refer the reader to Ganesan et al. (2014) and Lunt et al. (2016) for full details of the method as applied to atmospheric inversions. Here, we provide a brief overview of the method and the outline the specifics of the set-up as applied to this work. We solve for a state vector of emissions, $\mathbf{x}$, which are related to the data, $\mathbf{y}$, with the corresponding model values denoted by $\mathbf{H} \cdot \mathbf{x}$, where $\mathbf{x}$ denotes the state vector that includes emissions and boundary condition scaling factorsthrough the forward model in equation 2:

$$\mathbf{y} = \mathbf{H} \cdot \mathbf{x} + e, \tag{2}$$

where $\mathbf{H}$ is the sensitivity matrix, describing the response of atmospheric columns of CH_4 to changes in $\mathbf{x}$. The term e accounts for random errors in both model and measurements . in the forward model. In addition to solving for $\mathbf{x}$, the hierarchical Bayesian approach also takes into account uncertainties in the parameters, $\boldsymbol{\theta}$ that govern the form of the probability density function (PDF) of $\mathbf{x}$, such as the standard deviation for the case of a Gaussian PDF. The full form of the hierarchical Bayesian equation is given by:

$$\rho(\mathbf{x}, \boldsymbol{\theta}|\mathbf{y}) \propto \rho(\mathbf{y}|\mathbf{x}, \boldsymbol{\theta}) \cdot \rho(\mathbf{x}|\boldsymbol{\theta}) \cdot \rho(\boldsymbol{\theta}). \tag{3}$$

To estimate The ρ terms are used to denote a PDF. Equation 3 indicates that uncertainties in $\boldsymbol{\theta}$ propagate through to the *a posteriori* CH_4 fluxes from tropical Africa, we used a hierarchical Bayesian inversion using a Markov chain-Monte Carlo (MCMC) approach (Ganesan et al., 2014; Lunt et al., 2016). Bayesian inversions require that all quantities are described as probability density functions (PDFs) . The hierarchical MCMC approach allows hyper-parameters that describe these PDFs, such as model-measurement uncertainties , to be estimated as part of distribution of $\mathbf{x}$ on the left hand side of equation 3, which is one of the benefits of this approach given the inversion, reducing the impact of underlying assumptions. The approach also allows the *a priori* uncertainties to themselves be uncertain and explored in the inversion. A key benefit of this hierarchical MCMC approach is that uncertainties in the and model uncertainties may not be well known. In addition, the choice of *a priori* or measurement PDF is open to the investigator, which allows flexibility in cases where, for example, the PDF should be defined only on the positive axis. Since it cannot be solved analytically we estimate the *a posteriori* distribution are more representative of uncertainties in the inversion system, and any form of error variances can be used, provided they can be described by a PDF. of $\mathbf{x}$ using a Markov chain Monte Carlo (MCMC) approach.

At each step in the Markov chain a new state (e.g., new emissions parameter value) is proposed, based on the current value of the state. Whether that proposal is accepted or not depends on the following criterion:

$$U \leq \left(\frac{\rho(\mathbf{x}')}{\rho(\mathbf{x})} \times \frac{\rho(\mathbf{y}'|\mathbf{x}')}{\rho(\mathbf{y}|\mathbf{x})} \right), \tag{4}$$

where U is a ~~uniformally-distributed~~ uniformly-distributed random number between zero and one, and ρ represents a PDF. The term $\rho(\mathbf{x})$ represents the *a priori* PDF of the current state and $\rho(\mathbf{x}')$ the new proposed state. $\rho(\mathbf{y}|\mathbf{x})$ and $\rho(\mathbf{y}'|\mathbf{x}')$ represent the likelihood functions of the current and proposed states respectively. Consequently, the probability of a new proposal being accepted depends on the balance of the ratio between proposed and current *a priori* PDFs (how far the new state is from the *a priori*) and the likelihood ratio (how well it fits to the data).

This procedure is repeated many thousands of times to build up ~~a~~ an *a posteriori* PDF. ~~In our inversions, we ran the MCMC for 25~~

The state vector in this work is composed of terms representing scale factors applied to emissions, boundary conditions and initial conditions. We calculate the monthly emissions from a total of 38 regions across tropical Africa (Figure 1(b)). These regions are informed by national boundaries and major river basins or wetlands such as the Congo and Sudd. We include an additional six basis functions to describe monthly boundary condition scaling to the global CH_4 model field at the north, north-east, ~~000 iterations, the first 5,000 of which were discarded as a "burn-in" period. The resulting chain was thinned every 10th iteration to reduce storage, so that all a posterioridistributions contained 2,000 samples. Automatic tuning of proposal step sizes was performed during the burn-in period to ensure efficient ratios of acceptance between 20–50% (Tarantola, 2005). At every second iteration updates were proposed to all parameters in turn, and at iterations in between updates were proposed to the hyper-parameter values. A more comprehensive description of the hierarchical MCMC approach can be found in Ganesan et al. (2014) and Lunt et al. (2016).~~

south-east, south, south-west and north-west boundaries. We also include a basis function to describe the initial 3-D CH_4 mole fraction distribution within the nested domain at the start of the inversion period. In total, we calculated 3697 basis functions over our seven-year study period. We describe *a priori* distributions for each emissions basis function as a lognormal PDF, with an arithmetic standard deviation of 100%, reflecting the large uncertainty in the *a priori* estimates. *A priori* uncertainties on the boundary condition scaling factors were 0.5%, equivalent to a 10 ppb uncertainty on the mean value of each monthly field.

We use the uncertain parameters vector $\boldsymbol{\theta}$, to describe the model-measurement uncertainty that governs the form of the likelihood PDF, $\rho(\mathbf{y}|\mathbf{x},\boldsymbol{\theta})$, in equation 3. Model-measurement ~~errors~~ uncertainties were defined as a combination of the measurement uncertainties (which were fixed in the inversion) and a model uncertainty ~~component to be solved for in the inversion~~represented by the $\boldsymbol{\theta}$ parameters vector. The measurement uncertainty term represents the statistical uncertainties in the retrieved XCH_4 data, and averaged 9 ppb across all data points between 2010–~~2016. The~~ 2016 (Parker et al., 2015). The same measurement uncertainty values are used for both PR1 and PR2 data. The model uncertainty term was defined by a uniform distribution with lower and upper bounds of 5 ppb and 25 ppb respectively, with separate values estimated for model uncertainties in $8° \times 10°$ bins, and every month.

Due to the density of data, and to make the inversions more computationally tractable we assumed measurement errors were spatially and temporally uncorrelated. Although this might result in an underestimate of the posterior uncertainties, one approach to form a diagonal approximation of a full covariance matrix is through error inflation (Chevallier, 2007). The inclusion of a model uncertainty term in our inversions, in addition to the measurement uncertainty, partly acts to inflate the

error. In our inversions this term is allowed to vary, and constrained by the data, but is of a similar magnitude to the measurement uncertainty, with a mean a posteriori value of 8 ppb, leading to an increase in the error term. In addition, Turner et al. (2015) suggested that the measurement uncertainties of Parker et al. (2011) were already a conservative estimate of uncertainty, further adding to the observation error inflation.

The sensitivity matrix $\mathbf{H}$ was calculated by running the forward model for one month, with emissions in each basis function based on the *a priori* distribution. After one month the emissions were turned off and we tracked the 3-D CH_4 mole fraction field for a further three months as the signal decayed in the study domain due to atmospheric transport processes. After three months the residual signal due to perturbed emissions was negligible, so that we assumed zero sensitivity after this point. We sampled the model at the time and location of each GOSAT observed scene, and convolved the resulting model CH_4 profile with scene-dependent GOSAT averaging kernels to create the sensitivity matrix, $\mathbf{H}$.

In our inversions, we ran the MCMC for 25000 iterations, the first 5000 of which were discarded as a "burn-in" period. The resulting chain was thinned every 10th iteration to reduce storage, so that the *a posteriori* distribution of each element of the state vector contained 2000 samples. Automatic tuning of proposal step sizes was performed during the burn-in period to ensure efficient ratios of acceptance between 20–50% (Tarantola, 2005). Updates were proposed to all elements of $\mathbf{x}$ every second iteration. At iterations in between, updates were proposed to all the $\boldsymbol{\theta}$ values.

3 Results

We find the 2010–2016 mean *a posteriori* CH_4 emission estimate from tropical Africa is 76 (74–78) Tg yr^{-1} from the PR1 XCH_4 inversion, and 80 (78–82) Tg yr^{-1} from PR2 XCH_4. The numbers reported in brackets represent the 95% uncertainty range between the 2.5th and 97.5th percentiles of the *a posteriori* distribution. The difference between the estimates inferred from the PR1 and PR2 XCH_4, without any overlap considering the uncertainty range, clearly ~~show~~ shows how different assumptions in XCO_2 (equation 1) can impact the corresponding CH_4 emission estimates. The difference between PR1 and PR2 also indicates that the inability to account for these systematic uncertainties in the inversions leads to an underestimate of *a posteriori* uncertainty when using a single data product.

The difference between PR1 and PR2 inversions was largely due to differences in northern hemisphere tropical Africa (NH Africa) emissions. Mean PR2 emission estimates from each of the East, West and Central Africa regions, which are all largely or entirely contained in NH Africa, were each 2 Tg yr^{-1} larger than PR1 inversions. The mean NH Africa emissions from PR1 was 44 (42–45) Tg yr^{-1}, compared to 48 (47–50) Tg yr^{-1} from PR2. This is directly related to the differences between PR1 and PR2 XCH_4 data (Figure 2). The differences between our PR1 and PR2 emissions were greatest in 2010 due largely to West Africa emissions differences, consistent with the differences due to assumptions about $CO_{2\ model}$ shown in Figure 2. In contrast, mean *a posteriori* emissions from Southern Hemisphere Africa (SH Africa) between 2010 and 2016 were very similar with both PR1 and PR2 estimates of 32 (30–34) Tg yr^{-1}, reflecting a greater consistency of the underlying $CO_{2\ model}$ fields and hence proxy XCH_4 in SH Africa.

Our continental-scale results are consistent with previous estimates of African emissions from global CH_4 inversions. Saunois et al. (2016) report total African emissions in 2012, determined from a mean of 25 inversions, of 85 (70–106) Tg yr^{-1}. Our *a posteriori* estimates for 2012 were 73 (71–75) Tg yr^{-1} for PR1 and 77 (75–79) Tg yr^{-1} for PR2, although our study domain (Figure 1) does not include the extreme northern and southern regions of Africa. If we extrapolate our results to the African continent, based on the ratio of our *a priori* tropical African emissions to total continental Africa emissions of 90%, we estimate total African emissions of 81 (79–84) Tg yr^{-1} from PR1 and 85 (83–88) Tg yr^{-1} from PR2, ~~consistent with the results~~ well within the range of Saunois et al. (2016).

Figure 3 shows the 2010–2016 mean spatial distribution of our *a posteriori* CH_4 emissions estimates from PR1, the corresponding mean *a priori* emission distribution, and the difference between the two. Although emissions are shown at grid scale resolution of $0.5° \times 0.625°$, emissions were resolved using the coarser basis functions shown in Fig. 1(b), and the *a posteriori* fluxes are representative of these coarse scalings to the *a priori* grid scale distributions. We find consistent differences between the *a posteriori* distribution and *a priori* from certain areas in both PR1 (Figure 3) and PR2 inversions (not shown). For example, *a posteriori* emissions from East Africa (31 (30–33) Tg yr^{-1} for PR1 and 33 (31–34) Tg yr^{-1} for PR2) were almost twice as large as *a priori* emissions (17 Tg yr^{-1}) over the same region. East African *a posteriori* mean emissions account for 40% of the mean tropical African emissions in both PR1 and PR2 inversions. Our southern Africa *a posteriori* estimates (12 (11–14) Tg yr^{-1} for PR1 and PR2 inversions) were also larger than *a priori* emissions (7 Tg yr^{-1}).

~~In contrast~~This is further highlighted in Fig. 4, which shows the difference between the multi-year average *a posteriori* distributions from both PR1 and PR2 inversions and the *a priori* mean for each of the basis function regions. The *a priori* mean value lies outside the 95 percentile range for many of the distributions over the East African regions. In contrast, as shown in Fig. 3 and Fig. 4 we find significantly smaller 2010-2016 mean emissions over the Congo basin in Central Africa, particularly the central region of the basin known as the Cuvette Centrale. *A posteriori* emission estimates for PR1 (3.3 (2.7–4.0) Tg yr^{-1}) and PR2 (3.4 (2.7–4.1) Tg yr^{-1}) were very similar to each other and much smaller than the *a priori* emission estimate (8.5 Tg yr^{-1}). Wetland emissions accounted for more than 90% of *a priori* Congo Basin emissions, implying that the WetCHARTS ensemble mean used in the prior is an over-estimate of the wetland component of emissions in the Congo Basin. The WetCHARTS database provides a full multi-model ensemble of 324 models which have a large range of 2–21 Tg yr^{-1} for annual mean emissions from the Congo Basin and our *a posteriori* mean emissions for the region are more consistent with the models at the lower end of this range. This general finding of smaller *a posteriori* emissions ~~that~~ than WetCHARTS in the Congo is consistent with the spatial differences shown in Maasakkers et al. (2019). Our *a posteriori* estimate is more consistent with Tathy et al. (1992), who estimated methane emissions of 1.6–3.2 Tg yr^{-1} from the flooded forest zone of the Congo basin, based on static chamber measurements of methane flux.

3.1 Tropical African CH_4 Emission Trends

Figure 5(a) shows our *a posteriori* annual emission estimates from the tropical African region between 26°S–26°N. The results from the PR1 inversion indicate tropical African emissions increased from 72 (70–73) Tg in 2010 to 84 (82–86) Tg in 2016, with a mean positive trend in monthly emissions of +2.1 (1.7–2.5) Tg yr^{-1}. The PR2 estimates show a smaller difference

between 2010 and 2016, at 78 (76–80) Tg yr^{-1} and 84 (82–86) Tg yr^{-1} respectively, although there was a substantial dip in 2011 emissions. Consequently, the mean trend in monthly emissions for PR2 was smaller than PR1 but still positive, +1.5 (1.1–1.9) Tg yr^{-1}. This suggests that the overall pattern of increasing CH_4 emissions from tropical Africa is robust to assumptions about CO_2 made in the XCH_4 data.

Figure 5(b) shows the increase in tropical African emissions is driven mostly by emissions from East Africa in both inversions. Monthly *a posteriori* emissions from East Africa increased at a rate of +1.6 (1.3–1.9) Tg yr^{-1} in PR1 and +1.3 (1.0–1.6) Tg yr^{-1} in PR2, where the mean trend represents 80–90% of the total tropical Africa increase from the respective inversions. We found no consistent regional trends from the other African ~~reigon~~ region between the PR1 and PR2 inversions over the inversion period, although there was substantial inter-annual variability ~~,~~ which might mask any underlying trends particularly over West Africa, and both inversions show an increase of 4 (2–7) Tg yr^{-1} in Southern African emissions between 2014 and 2016.

We investigated the added benefit of including glint measurements by running a sensitivity calculation using only high-gain nadir measurements, which account for 75% of all observations. We designate these inversions $PR1_{nadir}$ and $PR2_{nadir}$. Mean emissions for the $PR1_{nadir}$ inversion were 75 (72–78) Tg yr^{-1} compared to 76 (74–78) Tg yr^{-1} from PR1, and the $PR2_{nadir}$ mean emissions were 80 (78–83) Tg yr^{-1} compared to 80 (78–82) Tg yr^{-1} from PR2. Therefore, when averaged over multiple years the differences were negligible. However, we find that omitting the glint data impacted the magnitude of the derived emission trends, with mean values 0.5–0.7 Tg yr^{-1} smaller than those inferred with both types of data at 1.4 (0.9–1.9) Tg yr^{-1} and 1.0 (0.5–1.5) Tg yr^{-1} for $PR1_{nadir}$ and $PR2_{nadir}$ respectively. This difference is due to greater constraint on the boundary condition terms in the inversions when using the glint observations (which are more sensitive to the ~~boundaries~~ scale factors applied to the domain boundaries due to their proximity to the edge of the domain). Whilst the trends in tropical African emissions from the nadir-only inversions between 2010–2016 are smaller, they remain positive and overlap within the uncertainty bounds with the PR1 and PR2 results. In common with the findings from PR1 and PR2 we find that 80–90% of the mean emissions trend can be explained by the mean trend in emissions from East Africa in the $PR1_{nadir}$ and $PR2_{nadir}$ inversions respectively.

To understand why East African CH_4 emissions play such an important role in the tropical African budget, we now examine the *a posteriori* emissions from more localized regions. Over East Africa, we find positive emission trends over a number of basis functions. However, given inter-annual variability and the *a posteriori* uncertainties in monthly emissions, the only basis function region that had a linear trend of monthly emissions with a p value less than 0.05 in both PR1 and PR2 inversions was in South Sudan, where the Sudd wetlands are located. For South Sudan, we find a linear trend of +0.4 Tg yr^{-1} (p=0.01) in both PR1 and PR2 inversions from this region. In the following section we present evidence that supports that this increase in emissions is associated with an increase in wetland emissions due to changes in the East African Lakes (Figure 1).

3.2 Annual Increases in South Sudanese CH_4 Emissions

Figure 6(a) shows annual CH_4 emission estimates from South Sudan between 2010–2016. Our *a posteriori* emissions in the PR1 inversion from the South Sudan region almost doubled from 3.1 (2.4–3.7) Tg yr^{-1} in 2010–2011 to 6.0 (5.2–6.9) Tg yr^{-1}

in 2015–2016. Similarly, for the PR2 inversion emissions increased from 3.4 (2.7–4.2) Tg yr^{-1} in 2010–2011 to 6.3 (5.4–7.2) Tg yr^{-1} in 2015–2016. Both inversions indicate a 3 Tg yr^{-1} increase of mean emissions during the inversion period, with a period of rapid growth between 2011 and 2014. Such a substantial increase in emissions in a short space of time implies a significant change to one or more CH_4 sources in this region.

The three main sources of CH_4 emissions in South Sudan in our *a priori* inventory are biomass burning, enteric fermentation from agriculture, and wetlands. GFED biomass burning estimates of CH_4 for 2010 are 30% smaller than subsequent years, largely due to a similar decrease in burned area in 2010 (not shown). Although the GFED CH_4 estimates therefore increase between 2010 and 2016, this cannot explain the large rise in emissions. *A priori* biomass burning emissions from GFED are estimated to be only 0.25 Tg yr^{-1} or 15% of annual *a priori* South Sudan emissions in 2016, and biomass burning emissions have a distinct seasonal cycle, peaking between November and February, while we observe a CH_4 emission increase in all seasons. Figure 6(b) shows that our annual South Sudanese CH_4 PR1 emission estimates are driven by changes in all seasons, but particularly in the wetter months between June–November. A similar pattern was found in the results from the PR2 inversion (not shown). Increased biomass burning may explain some contribution of the increasing emissions during December–February but it cannot explain increases at other times of the year.

Agricultural emissions from enteric fermentation ~~represents~~ represent another significant source in the *a priori* inventory for South Sudan, accounting for 25% of emissions. South Sudan does host a large livestock population but increased agricultural emissions are also unlikely to explain the inferred increased in CH_4 emissions. Based on IPCC emissions factors for African cattle of 31 kg $head^{-1}$ yr^{-1} (Eggleston et al., 2006), a 3 Tg yr^{-1} increase in emissions would require almost 100 million additional cattle to explain the increase, a population rise equivalent to the entire cattle stocks of the USA. Previous studies have highlighted that the emission factors adopted by the IPCC are highly uncertain and likely too low with values ranging from 31 kg $head^{-1}$ yr^{-1} to 62 kg $head^{-1}$ yr^{-1} for non-dairy cattle (Toit et al., 2014; Wolf et al., 2017; Kouazounde et al., 2014). Even assuming this upper limit for non-dairy cattle would still require an additional 50 million cattle to explain the rise in South Sudanese emissions. However, livestock estimates from the Food and Agricultural Organization of the United Nations (FAO, available at http://www.fao.org/faostat/) do not indicate a dramatic rise in livestock population, and we do not have any evidence to support the uniform adoption of a higher emission factor for enteric fermentation.

Wetlands are the major source of CH_4 in South Sudan, accounting for the remaining 60% of *a priori* emissions, of which the Sudd wetland, on the course of the White Nile, is the largest, with an area of 9,000–40,000 km^2 depending on the season (Rebelo et al., 2012). This wetland area represents a source of 0.8 Tg yr^{-1} in our *a priori* inventory, although our *a posteriori* mean suggests that these emissions are considerably larger (Figure 3), with our mean *a posteriori* estimates being 2.9 and 3.2 times larger than the prior in PR1 and PR2 respectively. To investigate how the Sudd might have changed during the inversion period we use land surface temperature (LST) data from the NASA Moderate Resolution Imaging Spectroradiometer (MODIS) as a proxy for wetland extent.

The use of satellite LST data ~~to infer information on~~ as a proxy for soil moisture is well-established ~~(e.g. Folwell et al., 2016; Gallego-Elv~~ ~~and can provide a proxy for wetland extent, since areas with~~ (e.g. Cammalleri and Vogt, 2015; Folwell et al., 2016; Gallego-Elvira et al., 20 . In dry conditions, evaporation of water from the soil is restricted, the ratio of latent heat to sensible heat flux decreases and thus

the surface temperature increases (Byrne et al., 1979). As such, areas of elevated soil moisture ~~should exhibit cooler~~ exhibit cooler surface temperatures than dry soil ~~, reducing the~~ and hence lower LST. The LST anomaly from the climatological monthly mean LST can thus provide a reasonable proxy for anomalies ~~from~~ of the mean seasonal cycle of wetland extent. MODIS pixels that are wetter than the climatological mean exhibit negative LST anomalies, and the temporal variation of these anomalies indicates the temporal variation in wetland extent. Data were used from both Terra and Aqua MODIS satellites, which have daytime equatorial crossing times of 1030 LT and 1330 LT respectively. To calculate wetland LST anomalies, we used monthly mean daytime-only LST data at 0.05 degree resolution (MOD11C3 and MYD11C3). We identified pixels prone to flooding where the minimum recorded January LST fell below 304 (306) K for Terra (Aqua). To create a monthly anomaly time series, we averaged LST over all of these wetland pixels having first subtracted their monthly climatological values (~~2003–2018~~2003–2018).

Figure 6(c) shows there was a significant decrease in MODIS LST anomalies over areas identified as seasonally flooded in the Sudd between 2010 and 2015, suggesting a growth in mean wetland extent. The decrease in LST anomaly is most pronounced during December—February and March-–May each year, with the seasonal anomalies decreasing by almost 8 K between 2010 and 2015. We find an insignificant trend in LST anomaly during September–November, when wetland extent is greatest. Interpretation of the seasonality of these trends requires some care. During June–November, soils throughout the region are wet, and this strongly suppresses LST, even in the absence of flooding. Moreover, cloud cover is increased during those months, which reduces the reliability of the LST data. The strong signals seen between December and May, when the methodology is expected to be most sensitive to interannual variability in flooding, provides clear evidence of an increase in wetland extent between 2010 and 2015 that helps to explain our increase in *a posteriori* CH_4 emissions. The LST data shown before 2010 back to 2007 indicates this was a transient event characterized by a particularly high December–May LST in 2010 (indicating a smaller wetland extent) followed by a trend to a minimum LST in 2015, and not indicative of a longer-term trend.

Our finding is consistent with previous works which have determined an increase in the spatial extent of the Sudd using MODIS LST diurnal temperature difference (Sosnowski et al., 2016), and MODIS land surface reflectance data (Vittorio and Georgakakos, 2018). Both studies indicate that the flooded extent of the Sudd was particularly small in 2009–2010 in both wet and dry seasons, with seasonally flooded vegetation that was constrained to be very close to the White Nile river itself. Vittorio and Georgakakos (2018) reports much greater flooded extents in 2012–2013 and shows an increase in dry season (yearly minimum) wetland extents of around 2000 km^2 between 2010 and 2014, related to changes in water flux into the Sudd.

Controls on the wetland extent of the Sudd are dominated by the inflow of water, as evapotranspiration rates exceed direct rainfall for the vast majority of the year (Sutcliffe and Brown, 2018). The inflow to the Sudd is a combination of outflow from the East African lakes (Victoria, Kyoga and Albert~~(~~, Figure 1), and seasonal variation provided by the runoff from streams in between Lake Albert and the Sudd called the torrents (Sutcliffe and Parks, 1999). The outflow from the East African lakes provides the medium-long term component of the Sudd inflow, while the torrents provide the seasonal peak flooding component. Our finding that *a posteriori* emissions from South Sudan increased at all times of year, together with the trend towards more negative LST anomalies during the dry season are more consistent with an increased upstream inflow from the East African lakes.

The influence of Lake Victoria water levels in particular on the extent of the Sudd has been well documented. Sutcliffe and Parks (1999) estimated that an increase in Lake Victoria water levels in the 1960s led to a trebling of permanent wetland extent in the Sudd, with a smaller effect on the increased extent of seasonal flooding. Recent outflow data from the East African lakes are not publicly available, but they can be approximated using the lake water levels. Since the 1950s the outflow of Lake Victoria has been controlled by at least one dam, which is regulated by an agreement with countries further downstream on the Nile basin called the Agreed Curve (Sene, 2000). This Agreed Curve is meant to mimic the natural relationship between outflow and lake level, although there is evidence that outflow rates from Lake Victoria far exceeded the Agreed Curve before lake levels reached a minimum in 2006 (e.g. Sutcliffe and Petersen, 2007; Owor et al., 2011; Vanderkelen et al., 2018). However, dam releases after this lake level minimum in 2006 have been shown to be more in line with the Agreed Curve (Owor et al., 2011).

Figure 6 (d) shows satellite altimetry data from Lake Victoria and Lake Albert from the Hydroweb database (Crétaux et al., 2011) between 2007 and 2016. The data show that Lake Victoria annual mean levels rose 0.6 m between 2010 and 2014 and Lake Albert levels rose by 0.8 m in this same period. The increased levels of both lakes imply an increased outflow from the East African lakes which is confirmed by Hydroweb altimetry data of the White Nile at 6.55 °N, 31.40 °E shown in Figure 6 (d). Annual mean water levels at this location at the southern end of the Sudd increased by 0.7 m between 2010 and 2014. Although this latter dataset is affected by variation of inflow to the Sudd due to the torrents, the data show increases of water level in the dry season as well as the wet, indicating the increased water levels at this location at the southern end of the Sudd are likely due to increased flow from further upstream as opposed to seasonal precipitation in the torrents.

In the absence of Lake Victoria outflow data it is possible the rise in lake water levels could be due to human management (through reduced dam releases). However, evaporation not outflow is the major loss process of water from the lake and the positive trends in altimetry data from further downstream at Lake Albert and in South Sudan indicate this explanation is unlikely, since they would not be consistent with a decrease in outflow. Furthermore, the recent increases in Lake Victoria water levels have been attributed to increased precipitation over the Lake Victoria basin (Awange et al., 2019). Whilst there may be no clear positive trend in monthly precipitation data from the Tropical Rainfall Measuring Mission (TRMM, Huffman et al., 2018), Figure 7 shows that increases in Lake Victoria seasonal water height anomalies and associated total terrestrial water storage generally follow large positive seasonal anomalies in precipitation over the lake catchment (delineated by the grey shading). The three years with largest annual precipitation totals over the Lake Victoria catchment between 2001–2016 were 2006, 2007 and 2011, which are all years that correspond to a subsequent increase in both lake levels and GRACE LWE anomalies. The data suggest that the positive precipitation anomalies over the Lake Victoria basin contributed to the rising lake levels and an increase in outflow is therefore likely. Together, the data from these multiple sources indicate increased inflow of the White Nile to the Sudd during the study period, which caused an increase in the extent of wetland flooding and a subsequent substantial increase in CH_4 emissions from South Sudan. In common with the LST anomaly data, the altimetry data before 2010 show that the period of rising water levels was largely confined to between 2010–2015, and indicate the transient nature of the increase in inflow and wetland extent, and the subsequent impact on CH_4 emissions from South Sudan.

3.3 Seasonal Variations of African CH_4 Emissions

Figure 8 shows the mean monthly climatological (2010–2016) CH_4 emissions from eight selected regions in both NH and SH Africa from the PR1 inversions. With the exception of the Congo basin, the emissions from all other regions shown in Fig. 8 are broadly correlated with the seasonal variation in GRACE LWE anomalies~~(~~. Chad, Sudan, South Sudan, Madagascar and the Niger Basin in particular show the strongest correlations with r^2 values of ~~0.2–0.8).~~ 0.7 as shown in Fig. 8. Seasonal variations of *a posteriori* CH_4 emissions in most regions are not strongly related to changes in surface skin temperature, which is another parameter commonly used in models to help describe the temporal variation of wetland CH_4 emissions (e.g. Gedney, 2004). Seasonal variations in emissions from biomass burning (the timing of which is shown by burned area in Figure 8) are generally much smaller than the inferred seasonal cycle of emissions. The exceptions are the South Sudan and Angola/Zambia regions. There are two peaks in the seasonal cycle of emissions from South Sudan, the second of which in December coincides with the peak in burned area and associated biomass burning emissions. Similarly in Angola/Zambia there is a noticeable but small emissions peak between July–September when burned area is at a maximum.

Correlations between the seasonality of tropical wetland methane emissions and GRACE LWE anomaly data water storage from GRACE has been previously reported (e.g. Bloom et al., 2010, 2012). Some of the areas shown in Figure 8 contain significant wetland regions: in South Sudan the Sudd; in Niger Basin the Niger Inland delta; and in Angola/Zambia the Barotse floodplain. Estimates of seasonal wetland extent of the Sudd, suggest that it is composed of around 20% permanent and 80% seasonally flooded wetlands (Rebelo et al., 2012), and as such a large seasonal cycle of CH_4 emissions in this region is expected. Similarly, for the Barotse floodplain in Angola/Zambia, past work has estimated an inundated wetland extent that is approximately ten times larger at its peak compared to the dry season minimum (Zimba et al., 2018). Our 2010–2016 mean *a posteriori* seasonal cycle of CH_4 emissions for the Angola/Zambia region (containing the Barotse floodplain) has a peak in January–February that is around 3 times larger than the minimum in October in both PR1 and PR2 inversions, although this region includes emissions from more than this single wetland area.

Taylor et al. (2018) used the Global Inundation Extent from Multi-Satellites (GIEMS, Prigent et al., 2007, 2012) dataset to identify those wetlands with the greatest seasonal variation in extent, highlighting the Barotse floodplains, the Niger Inland delta and an area to the South of Lake Chad as being most significant. The timing of maximum wetland extent was shown to be largely driven by the seasonal migration of the Intertropical Convergence Zone (ITCZ), with peak extents in NH Africa typically around October. Figure 8 shows the seasonal peak in our *a posteriori* northern hemisphere emission regions (panels (a)–(e)) occurs consistently between September and November. If we assume that this is largely driven by the seasonal cycle of wetlands then the timing of our *a posteriori* emissions peak is more consistent with the findings of Bloom et al. (2012), inferred from SCIAMACHY XCH_4 data, where northern tropical Africa emissions peak between September–November, compared to the later work of Bloom et al. (2017) in which the seasonal cycle peaks earlier in April–October.

We acknowledge that the large inferred seasonal cycles shown in Figure 8 may not reflect exclusively changes in wetland emissions. Based on production estimates, rice paddy emissions will follow a similar seasonal cycle (Laborte et al., 2017),

although emissions from rice comprise only 4% of the *a priori* anthropogenic component of tropical African emissions, and are largely concentrated in West Africa. In addition, the contribution of livestock enteric fermentation emissions to the seasonal CH_4 emission cycle cannot be discounted. In the semi-arid ecosystems of sub-Saharan Africa, ecosystem productivity is strongly linked to soil moisture (Madani et al., 2017). Studies of sub-Saharan cattle have shown that animal weights and dry matter intake vary seasonally, linked to the availability of forage (Ayantunde et al., 2005; Assouma et al., 2018). As such, the seasonal variation of enteric fermentation CH_4 emissions from livestock could be a significant contributor to the seasonal cycle of total CH_4 emissions that we infer. One potential indicator of this is that we infer large seasonal cycles in regions that contain the largest livestock populations, such as Ethiopia and Sudan. The magnitude of the seasonal cycle in Ethiopia is comparable to that of South Sudan, despite the former not containing seasonal wetlands of the extent of the Sudd. However, since we are limited to resolving emissions at broad scales, and both agricultural and wetland sources have similar spatial distributions across Africa, we are unable to quantify the relative contributions of different sources to the seasonal cycle.

Our results for the Congo Basin show no evidence of a significant water storage dependent seasonal cycle of CH_4 emissions. The Congo basin straddles the equator and therefore experiences two wet seasons each year, in March and October (Figure 8). The central part of the basin, referred to as the Cuvette Centrale, is permanently flooded, largely rain-fed and contains large stores of peat (Dargie et al., 2017). These features are consistent with a muted seasonal cycle of CH_4 emissions. In contrast with the *a priori* emissions we use from WetCHARTs ensemble mean, which have an average peak-to-peak seasonal cycle magnitude of around 4 Tg yr^{-1}, our *a posteriori* emissions mean peak-to-peak seasonal cycle is $\simeq$1 Tg yr^{-1}. This seasonal cycle magnitude is smaller than the mean monthly 95% uncertainty range on the *a posteriori* estimates. Our results from the Congo Basin are consistent with the results reported by Parker et al. (2018), who identified a smaller peak-to-peak seasonal cycle in GOSAT XCH_4 data compared to the XCH_4 predicted by the WetCHARTs ensemble mean.

3.4 Sensitivity to model bias correction

In addition to the sensitivity to different proxy XCH_4 datasets, we also tested the sensitivity of our results to a bias in the GEOS-Chem model that has previously been reported for CH_4 (Turner et al., 2015; Maasakkers et al., 2019). We applied the quadratic regression bias correction $y = 0.005 \times (\lambda^2 - \lambda - 100))$ from Turner et al. (2015) to the PR1 data and performed a new set of inversions, (referred to as $PR1_{BC}$) where λ is the latitude in degrees, and y the bias term. The bias correction was around 3 ppb at the north and south boundaries of our tropical domain, tending to –0.5 ppb at the equator.

The results of this bias corrected inversion show the mean total African emissions to be 72 (70–74) Tg yr^{-1}, compared to 76 (74–78) Tg yr^{-1} in the non-bias corrected PR1 inversion. The difference in total African emissions is equivalent to the difference between PR1 and PR2 inversions, albeit with smaller total emissions when the bias correction was applied. The trend in tropical African emissions in the $PR1_{BC}$ inversion was 2.0 (1.6–2.4) Tg yr^{-1}, compared to 2.1 (1.7–2.5) Tg yr^{-1} in the PR1 inversion. In common with the PR1 inversion the trend in East African emissions was also 1.7 (1.4–2.0) Tg yr^{-1} in $PR1_{BC}$. Emissions from the Sudd were found to have increased at a rate of 0.3 Tg yr^{-1} in $PR1_{BC}$. As such, our main conclusions in this work are robust to the presence of a small latitudinally dependent bias in the GEOS-Chem simulation of CH_4. We propose

this is because the presence of any latitudinal bias can be largely subsumed into the boundary conditions scaling in the regional inversion, minimizing the impacts of a potential model transport bias.

4 Concluding Remarks

We use GOSAT proxy XCH_4 data and a nested version of the GEOS-Chem atmospheric chemistry transport model to infer emissions of CH_4 over tropical Africa. At the heart of this data product is the ratio of XCH_4:XCO_2, which effectively minimizes spectral artifacts due to cloud and aerosol scattering. A model estimate of XCO_2 is typically used to infer a proxy retrieval of XCH_4. In this work, we use two XCO_2 model estimates: 1) an ensemble mean of three independent models (including GEOS-Chem) denoted as PR1; and 2) GEOS-Chem fields that have been fitted to GOSAT XCO_2 denoted as PR2. Mean *a posteriori* tropical African emission estimates for 2010–2016 are 76 (74–78) Tg yr^{-1} and 80 (78–82) Tg yr^{-1} for PR1 and PR2, respectively. Our results illustrate the sensitivity of *a posteriori* CH_4 emissions on our choice of XCO_2 to determine the proxy XCH_4 data product. Here, the difference is driven by a seasonal cycle of CO_2 fluxes over northern tropical Africa inferred from GOSAT that is larger than that inferred by *in situ* data.

Our *a posteriori* CH_4 emissions represent 15% of the global emissions estimate of 546 Tg yr^{-1} in Maasakkers et al. (2019) derived from GOSAT data between 2010 and 2015. Whilst they represent a significant fraction of the global budget, changes over tropical Africa are unlikely to be exclusively responsible for observed global-scale variations. We find a mean emissions trend of 2.1 (1.7–2.5) Tg yr^{-1} from PR1 and 1.5 (1.1–1.9) Tg yr^{-1} from PR2 between 2010 and 2016, representing around a third of the global growth trend in emissions during this period from global inversions. McNorton et al. (2018) reported a global growth rate between 2007–2015 of 5.7$\pm$0.8 Tg yr^{-1}. Thompson et al. (2018) found an increase in global microbial sources of 24–48 Tg yr^{-1} between 2006–2014 mostly originating from tropical latitudes, equivalent to a global growth rate of 3–6 Tg yr^{-1}. Although Saunois et al. (2017) found emissions from the tropics to have increased by 18 (13–24) Tg yr^{-1} between the periods 2002–2006 and 2008–2012, relatively little of this was ascribed to Africa. This is qualitatively consistent with our hypothesis that the increase in emissions from East African regions, and in particular the Sudd, due to increased water levels of the East African lakes was limited to the period between 2010 and 2016. Moreover, previous studies have tended to focus on large continental regions when investigating trends in CH_4, which may mask any smaller regional changes that are only apparent through inspecting finer-scale spatial distributions. For comparison to other global regions, our *a posteriori* trend for tropical Africa is larger than those recently reported for China of 1.1 (0.7–1.5) Tg yr^{-1} and India (0.7 (0.2–1.2) Tg yr^{-1}) between 2010 and 2015 (Miller et al., 2019).

We attribute a large part of the increase in African emissions between 2010 and 2016 to the increasing wetland extent of the Sudd, driven largely by increased water levels in the upstream East African lakes. Emissions from the Sudd wetlands are found to have increased during the study period by 3 Tg yr^{-1}. However, satellite altimetry data shows a stabilisation of the East African lake levels after 2014, and LST anomaly data, used as a proxy for wetland extent, suggest the trend of increasing Sudd wetland extent only lasted between 2010–2015, and that the wetland extent was anomalously small in 2010. Our *a posteriori* emission estimates also suggest a stabilisation of emissions in 2015–2016, indicating that the increase in emissions from the

Sudd was a transient event. No other easily identifiable wetland areas were estimated to have a significant growth in emissions between 2010 and 2016. Continental-scale atmospheric isotopic $^{13}CH_4$ data show a shift towards lighter values, which have been used to suggest an increase in tropical microbial emissions since 2007 (Nisbet et al., 2016; Schaefer et al., 2016). Our findings over South Sudan are not inconsistent with this hypothesis. Although our inversions do not distinguish between different emission source of CH_4, the location and trends in satellite LST and altimetry data suggest this increase was due to wetland emissions from the Sudd. FAO estimates of livestock population and IPCC Tier 1 emission factors also suggest a modest increase in agricultural emissions from the wider East Africa region of 0.2 Tg yr^{-1}, which would also be qualitatively consistent with the trends in isotope signals.

Our *a posteriori* emission estimates show that CH_4 emissions across tropical Africa are highly seasonal, with the peak in monthly emissions of each hemisphere strongly correlated with the peak in ground water storage. Whilst the link between water storage and wetland CH_4 emissions is well established, the lack of a seasonal cycle of emissions in the Congo Basin highlights that this linkage is not uniform across all tropical wetlands. Furthermore, the presence of a large seasonal cycle in regions such as Ethiopia where livestock are likely to be the dominant source may indicate seasonality in other CH_4 sources. However, emissions were resolved using coarse basis functions largely at national scales and at monthly timescales which do not allow us to separate out the contribution of different sources. Future studies using higher resolution data from satellites such as TROPOMI may help to better understand the temporal and spatial characteristics of the seasonal cycle of methane emissions from both wetlands and other sources. Indeed, initial data from TROPOMI appears promising in isolating large wetland systems such as the Sudd (Hu et al., 2018), which should enhance the future monitoring of this large CH_4 source region. Incorporating additional information from complementary measurement data into the inversion system could further help to reduce uncertainties in the CH_4 budget. Examples of potentially useful space-based measurements include formaldehyde to constrain the temporal and spatial variability of the OH radical sink (Wolfe et al., 2019), and GRACE data (and its follow-on mission) to help constrain the temporal variability of wetland emissions.

Satellite observations now play an integral role in observing and monitoring land, ocean, and atmospheric components of the global carbon cycle (Palmer, 2018). As these data become available at progressively higher spatial resolution, we can begin to address scientific questions that focus on understanding how different ecosystems ~~changes~~ change with climate. However, the value of these data disproportionately increases with the availability and integration of *in situ* atmospheric and ecological data that provide complementary detailed information on finer spatial and temporal scales.

Data availability. UoL GOSAT satellite column observations of CH_4 are available for download from the Centre for Environmental Data Analysis, http://catalogue.ceda.ac.uk/uuid/f9154243fd8744bdaf2a59c39033e659.

Code and data availability. The GEOS-Chem model is a community model and is freely available (http://acmg.seas.harvard.edu/geos/). The model metadata is freely available.

Author contributions. MFL and PIP designed the experiments, and MFL performed all calculations. MFL wrote the paper with contributions from PIP. LF provided global CH_4 and CO_2 inversion outputs. CMT provided inputs on the hydrological cycle and LST over tropical Africa. HB and RJP provided access to the GOSAT XCH_4 data. All coauthors provided comments on the manuscript.

Competing interests. The authors declare no conflicts of interest.

Acknowledgements. MFL and PIP gratefully acknowledge funding from the Methane Observations and Yearly Assessments (MOYA) project funded by the National Environment Research Council (NERC, grant #NE/N015916/1). PIP, HB, RJP and CMT acknowledge support from the UK National Centre for Earth Observation (NCEO). NERC provides national capability funding to NCEO (grant #PR140015). HB and RJP acknowledge funding from Copernicus C3S and ESA CCI.

References

Assouma, M., Lecomte, P., Hiernaux, P., Ickowicz, A., Corniaux, C., Decruyenaere, V., Diarra, A., and Vayssières, J.: How to better account for livestock diversity and fodder seasonality in assessing the fodder intake of livestock grazing semi-arid sub-Saharan Africa rangelands, Livestock Science, 216, 16–23, https://doi.org/10.1016/j.livsci.2018.07.002, 2018.

Awange, J., Saleem, A., Sukhadiya, R., Ouma, Y., and Kexiang, H.: Physical dynamics of Lake Victoria over the past 34 years (1984–2018): Is the lake dying?, Science of The Total Environment, 658, 199–218, https://doi.org/10.1016/j.scitotenv.2018.12.051, 2019.

Ayantunde, A., Fernández-Rivera, S., and McCrabb, G., eds.: Coping with feed scarcity in smallholder livestock systems in developing countries, International Livestock Research Institute (ILRI), 2005.

Bergamaschi, P., Frankenberg, C., Meirink, J. F., Krol, M., Dentener, F., Wagner, T., Platt, U., Kaplan, J. O., Körner, S., Heimann, M., Dlugokencky, E. J., and Goede, A.: Satellite chartography of atmospheric methane from SCIAMACHY on board ENVISAT: 2. Evaluation based on inverse model simulations, Journal of Geophysical Research, 112, https://doi.org/10.1029/2006jd007268, 2007.

Bey, I., Jacob, D. J., Yantosca, R. M., Logan, J. A., Field, B. D., Fiore, A. M., Li, Q., Liu, H. Y., Mickley, L. J., and Schultz, M. G.: Global modeling of tropospheric chemistry with assimilated meteorology: Model description and evaluation, Journal of Geophysical Research: Atmospheres, 106, 23 073–23 095, https://doi.org/10.1029/2001jd000807, 2001.

Bloom, A. A., Palmer, P. I., Fraser, A., Reay, D. S., and Frankenberg, C.: Large-Scale Controls of Methanogenesis Inferred from Methane and Gravity Spaceborne Data, Science, 327, 322–325, https://doi.org/10.1126/science.1175176, 2010.

Bloom, A. A., Palmer, P. I., Fraser, A., and Reay, D. S.: Seasonal variability of tropical wetland CH_4 emissions: the role of the methanogen-available carbon pool, Biogeosciences, 9, 2821–2830, https://doi.org/10.5194/bg-9-2821-2012, 2012.

Bloom, A. A., Bowman, K. W., Lee, M., Turner, A. J., Schroeder, R., Worden, J. R., Weidner, R., McDonald, K. C., and Jacob, D. J.: A global wetland methane emissions and uncertainty dataset for atmospheric chemical transport models (WetCHARTs version 1.0), Geoscientific Model Development, 10, 2141–2156, https://doi.org/10.5194/gmd-10-2141-2017, 2017.

Bosilovich, M. G., Lucchesi, R., and Suarez, M.: MERRA-2: File Specification, Tech. Rep. 9, v1.1, Global Modeling and Assimilation Office, NASA Goddard Space Flight Center, http://gmao.gsfc.nasa.gov/pubs/office_notes, 2016.

Byrne, G. F., Begg, J. E., Fleming, P. M., and Dunin, F. X.: Remotely sensed land cover temperature and soil water status—a brief review, Remote Sensing of Environment, 8, 291–305, https://doi.org/10.1016/0034-4257(79)90029-4, 1979.

Cammalleri, C. and Vogt, J.: On the Role of Land Surface Temperature as Proxy of Soil Moisture Status for Drought Monitoring in Europe, Remote Sensing, 7, 16 849–16 864, https://doi.org/10.3390/rs71215857, 2015.

Chevallier, F.: Impact of correlated observation errors on inverted CO2surface fluxes from OCO measurements, Geophysical Research Letters, 34, https://doi.org/10.1029/2007gl030463, 2007.

Crétaux, J.-F., Jelinski, W., Calmant, S., Kouraev, A., Vuglinski, V., Bergé-Nguyen, M., Gennero, M.-C., Nino, F., Rio, R. A. D., Cazenave, A., and Maisongrande, P.: SOLS: A lake database to monitor in the Near Real Time water level and storage variations from remote sensing data, Advances in Space Research, 47, 1497–1507, https://doi.org/10.1016/j.asr.2011.01.004, 2011.

Crutzen, P. J., Aselmann, I., and Seiler, W.: Methane production by domestic animals, wild ruminants, other herbivorous fauna, and humans, Tellus B, 38B, 271–284, https://doi.org/10.1111/j.1600-0889.1986.tb00193.x, 1986.

Dargie, G. C., Lewis, S. L., Lawson, I. T., Mitchard, E. T. A., Page, S. E., Bocko, Y. E., and Ifo, S. A.: Age, extent and carbon storage of the central Congo Basin peatland complex, Nature, 542, 86–90, https://doi.org/10.1038/nature21048, 2017.

Eggleston, H., Buendia, L., Miwa, K., Ngara, T., and Tanabe, K., eds.: 2006 IPCC Guidelines for National Greenhouse Gas Inventories, Prepared by the National Greenhouse Gas Inventories Programme, IGES, Japan, 2006.

Feng, L., Palmer, P. I., Parker, R. J., Deutscher, N. M., Feist, D. G., Kivi, R., Morino, I., and Sussmann, R.: Estimates of European uptake of CO_2 inferred from GOSAT XCO_2 retrievals: sensitivity to measurement bias inside and outside Europe, Atmospheric Chemistry and Physics, 16, 1289–1302, https://doi.org/10.5194/acp-16-1289-2016, 2016.

Feng, L., Palmer, P. I., Bösch, H., Parker, R. J., Webb, A. J., Correia, C. S. C., Deutscher, N. M., Domingues, L. G., Feist, D. G., Gatti, L. V., Gloor, E., Hase, F., Kivi, R., Liu, Y., Miller, J. B., Morino, I., Sussmann, R., Strong, K., Uchino, O., Wang, J., and Zahn, A.: Consistent regional fluxes of CH_4 and CO_2 inferred from GOSAT proxy $XCH_4 : XCO_2$ retrievals, 2010–2014, Atmospheric Chemistry and Physics, 17, 4781–4797, https://doi.org/10.5194/acp-17-4781-2017, 2017.

Folwell, S. S., Harris, P. P., and Taylor, C. M.: Large-Scale Surface Responses during European Dry Spells Diagnosed from Land Surface Temperature, Journal of Hydrometeorology, 17, 975–993, https://doi.org/10.1175/jhm-d-15-0064.1, 2016.

Frankenberg, C., Aben, I., Bergamaschi, P., Dlugokencky, E. J., van Hees, R., Houweling, S., van der Meer, P., Snel, R., and Tol, P.: Global column-averaged methane mixing ratios from 2003 to 2009 as derived from SCIAMACHY: Trends and variability, Journal of Geophysical Research: Atmospheres, 116, https://doi.org/10.1029/2010JD014849, 2011.

Fraser, A., Palmer, P. I., Feng, L., Boesch, H., Cogan, A., Parker, R., Dlugokencky, E. J., Fraser, P. J., Krummel, P. B., Langenfelds, R. L., O'Doherty, S., Prinn, R. G., Steele, L. P., van der Schoot, M., and Weiss, R. F.: Estimating regional methane surface fluxes: the relative importance of surface and GOSAT mole fraction measurements, Atmospheric Chemistry and Physics, 13, 5697–5713, https://doi.org/10.5194/acp-13-5697-2013, 2013.

Fung, I., John, J., Lerner, J., Matthews, E., Prather, M., Steele, L. P., and Fraser, P. J.: Three-dimensional model synthesis of the global methane cycle, Journal of Geophysical Research, 96, 13 033, https://doi.org/10.1029/91jd01247, 1991.

Gallego-Elvira, B., Taylor, C. M., Harris, P. P., Ghent, D., Veal, K. L., and Folwell, S. S.: Global observational diagnosis of soil moisture control on the land surface energy balance, Geophysical Research Letters, 43, 2623–2631, https://doi.org/10.1002/2016gl068178, 2016.

Ganesan, A. L., Rigby, M., Zammit-Mangion, A., Manning, A. J., Prinn, R. G., Fraser, P. J., Harth, C. M., Kim, K.-R., Krummel, P. B., Li, S., Mühle, J., O'Doherty, S. J., Park, S., Salameh, P. K., Steele, L. P., and Weiss, R. F.: Characterization of uncertainties in atmospheric trace gas inversions using hierarchical Bayesian methods, Atmospheric Chemistry and Physics, 14, 3855–3864, https://doi.org/10.5194/acp-14-3855-2014, 2014.

Ganesan, A. L., Rigby, M., Lunt, M. F., Parker, R. J., Boesch, H., Goulding, N., Umezawa, T., Zahn, A., Chatterjee, A., Prinn, R. G., Tiwari, Y. K., van der Schoot, M., and Krummel, P. B.: Atmospheric observations show accurate reporting and little growth in India's methane emissions, Nature Communications, 8, https://doi.org/10.1038/s41467-017-00994-7, 2017.

Gedney, N.: Climate feedback from wetland methane emissions, Geophysical Research Letters, 31, https://doi.org/10.1029/2004gl020919, 2004.

Gedney, N. and Cox, P. M.: The Sensitivity of Global Climate Model Simulations to the Representation of Soil Moisture Heterogeneity, Journal of Hydrometeorology, 4, 1265–1275, https://doi.org/10.1175/1525-7541(2003)004<1265:tsogcm>2.0.co;2, 2003.

Goopy, J., Onyango, A., Dickhoefer, U., and Butterbach-Bahl, K.: A new approach for improving emission factors for enteric methane emissions of cattle in smallholder systems of East Africa – Results for Nyando, Western Kenya, Agricultural Systems, 161, 72–80, https://doi.org/10.1016/j.agsy.2017.12.004, 2018.

Gumbricht, T., Roman-Cuesta, R. M., Verchot, L., Herold, M., Wittmann, F., Householder, E., Herold, N., and Murdiyarso, D.: An expert system model for mapping tropical wetlands and peatlands reveals South America as the largest contributor, Global Change Biology, 23, 3581–3599, https://doi.org/10.1111/gcb.13689, https://onlinelibrary.wiley.com/doi/abs/10.1111/gcb.13689, 2017.

Hausmann, P., Sussmann, R., and Smale, D.: Contribution of oil and natural gas production to renewed increase in atmospheric methane (2007–2014): top–down estimate from ethane and methane column observations, Atmospheric Chemistry and Physics, 16, 3227–3244, https://doi.org/10.5194/acp-16-3227-2016, 2016.

Houweling, S., Baker, D., Basu, S., Boesch, H., Butz, A., Chevallier, F., Deng, F., Dlugokencky, E. J., Feng, L., Ganshin, A., Hasekamp, O., Jones, D., Maksyutov, S., Marshall, J., Oda, T., O'Dell, C. W., Oshchepkov, S., Palmer, P. I., Peylin, P., Poussi, Z., Reum, F., Takagi, H., Yoshida, Y., and Zhuravlev, R.: An intercomparison of inverse models for estimating sources and sinks of CO2 using GOSAT measurements, Journal of Geophysical Research: Atmospheres, 120, 5253–5266, https://doi.org/10.1002/2014JD022962, https://agupubs.onlinelibrary.wiley.com/doi/abs/10.1002/2014JD022962, 2015.

Hu, H., Landgraf, J., Detmers, R., Borsdorff, T., de Brugh, J. A., Aben, I., Butz, A., and Hasekamp, O.: Toward Global Mapping of Methane With TROPOMI: First Results and Intersatellite Comparison to GOSAT, Geophysical Research Letters, 45, 3682–3689, https://doi.org/10.1002/2018gl077259, 2018.

Huffman, G., Stocker, E., Bolvin, D., and Nelkin, E.: TRMM (TMPA/3B43) Rainfall Estimate L3 1 month 0.25 degree x 0.25 degree V7, https://doi.org/10.5067/trmm/tmpa/month/7, 2018.

Janssens-Maenhout, G., Crippa, M., Guizzardi, D., Muntean, M., Schaaf, E., Dentener, F., Bergamaschi, P., Pagliari, V., Olivier, J. G. J., Peters, J. A. H. W., van Aardenne, J. A., Monni, S., Doering, U., and Petrescu, A. M. R.: EDGAR v4.3.2 Global Atlas of the three major Greenhouse Gas Emissions for the period 1970–2012, Earth System Science Data Discussions, pp. 1–55, https://doi.org/10.5194/essd-2017-79, 2017.

Kirschke, S., Bousquet, P., Ciais, P., Saunois, M., Canadell, J. G., Dlugokencky, E. J., Bergamaschi, P., Bergmann, D., Blake, D. R., Bruhwiler, L., Cameron-Smith, P., Castaldi, S., Chevallier, F., Feng, L., Fraser, A., Heimann, M., Hodson, E. L., Houweling, S., Josse, B., Fraser, P. J., Krummel, P. B., Lamarque, J.-F., Langenfelds, R. L., Quéré, C. L., Naik, V., O'Doherty, S., Palmer, P. I., Pison, I., Plummer, D., Poulter, B., Prinn, R. G., Rigby, M., Ringeval, B., Santini, M., Schmidt, M., Shindell, D. T., Simpson, I. J., Spahni, R., Steele, L. P., Strode, S. A., Sudo, K., Szopa, S., van der Werf, G. R., Voulgarakis, A., van Weele, M., Weiss, R. F., Williams, J. E., and Zeng, G.: Three decades of global methane sources and sinks, Nature Geoscience, 6, 813–823, https://doi.org/10.1038/ngeo1955, 2013.

Kouazounde, J. B., Gbenou, J. D., Babatounde, S., Srivastava, N., Eggleston, S. H., Antwi, C., Baah, J., and McAllister, T. A.: Development of methane emission factors for enteric fermentation in cattle from Benin using IPCC Tier 2 methodology, animal, 9, 526–533, https://doi.org/10.1017/s1751731114002626, 2014.

Kuze, A., Suto, H., Nakajima, M., and Hamazaki, T.: Thermal and near infrared sensor for carbon observation Fourier-transform spectrometer on the Greenhouse Gases Observing Satellite for greenhouse gases monitoring, Applied Optics, 48, 6716, https://doi.org/10.1364/ao.48.006716, 2009.

Laborte, A. G., Gutierrez, M. A., Balanza, J. G., Saito, K., Zwart, S. J., Boschetti, M., Murty, M., Villano, L., Aunario, J. K., Reinke, R., Koo, J., Hijmans, R. J., and Nelson, A.: RiceAtlas, a spatial database of global rice calendars and production, Scientific Data, 4, 170 074, https://doi.org/10.1038/sdata.2017.74, 2017.

Lehner, B. and Doll, P.: Development and validation of a global database of lakes, reservoirs and wetlands, Journal of Hydrology, 296, 1–22, https://doi.org/10.1016/j.jhydrol.2004.03.028, 2004.

Lunt, M. F., Rigby, M., Ganesan, A. L., and Manning, A. J.: Estimation of trace gas fluxes with objectively determined basis functions using reversible-jump Markov chain Monte Carlo, Geoscientific Model Development, 9, 3213–3229, https://doi.org/10.5194/gmd-9-3213-2016, 2016.

Maasakkers, J. D., Jacob, D. J., Sulprizio, M. P., Scarpelli, T. R., Nesser, H., Sheng, J.-X., Zhang, Y., Hersher, M., Bloom, A. A., Bowman, K. W., Worden, J. R., Janssens-Maenhout, G., and Parker, R. J.: Global distribution of methane emissions, emission trends, and OH concentrations and trends inferred from an inversion of GOSAT satellite data for 2010–2015, Atmospheric Chemistry and Physics, 19, 7859–7881, https://doi.org/10.5194/acp-19-7859-2019, 2019.

Madani, N., Kimball, J., Jones, L., Parazoo, N., and Guan, K.: Global Analysis of Bioclimatic Controls on Ecosystem Productivity Using Satellite Observations of Solar-Induced Chlorophyll Fluorescence, Remote Sensing, 9, 530, https://doi.org/10.3390/rs9060530, 2017.

McNorton, J., Gloor, E., Wilson, C., Hayman, G. D., Gedney, N., Comyn-Platt, E., Marthews, T., Parker, R. J., Boesch, H., and Chipperfield, M. P.: Role of regional wetland emissions in atmospheric methane variability, Geophysical Research Letters, 43, 11,433–11,444, https://doi.org/10.1002/2016gl070649, 2016.

McNorton, J., Wilson, C., Gloor, M., Parker, R. J., Boesch, H., Feng, W., Hossaini, R., and Chipperfield, M. P.: Attribution of recent increases in atmospheric methane through 3-D inverse modelling, Atmospheric Chemistry and Physics, 18, 18 149–18 168, https://doi.org/10.5194/acp-18-18149-2018, 2018.

Melton, J. R., Wania, R., Hodson, E. L., Poulter, B., Ringeval, B., Spahni, R., Bohn, T., Avis, C. A., Beerling, D. J., Chen, G., Eliseev, A. V., Denisov, S. N., Hopcroft, P. O., Lettenmaier, D. P., Riley, W. J., Singarayer, J. S., Subin, Z. M., Tian, H., Zürcher, S., Brovkin, V., van Bodegom, P. M., Kleinen, T., Yu, Z. C., and Kaplan, J. O.: Present state of global wetland extent and wetland methane modelling: conclusions from a model inter-comparison project (WETCHIMP), Biogeosciences, 10, 753–788, https://doi.org/10.5194/bg-10-753-2013, 2013.

Miller, S. M., Michalak, A. M., Detmers, R. G., Hasekamp, O. P., Bruhwiler, L. M. P., and Schwietzke, S.: China's coal mine methane regulations have not curbed growing emissions, Nature Communications, 10, https://doi.org/10.1038/s41467-018-07891-7, 2019.

Murray, L. T., Jacob, D. J., Logan, J. A., Hudman, R. C., and Koshak, W. J.: Optimized regional and interannual variability of lightning in a global chemical transport model constrained by LIS/OTD satellite data, Journal of Geophysical Research: Atmospheres, 117, https://doi.org/10.1029/2012jd017934, 2012.

Nisbet, E. G., Dlugokencky, E. J., and Bousquet, P.: Methane on the Rise–Again, Science, 343, 493–495, https://doi.org/10.1126/science.1247828, 2014.

Nisbet, E. G., Dlugokencky, E. J., Manning, M. R., Lowry, D., Fisher, R. E., France, J. L., Michel, S. E., Miller, J. B., White, J. W. C., Vaughn, B., Bousquet, P., Pyle, J. A., Warwick, N. J., Cain, M., Brownlow, R., Zazzeri, G., Lanoisellé, M., Manning, A. C., Gloor, E., Worthy, D. E. J., Brunke, E.-G., Labuschagne, C., Wolff, E. W., and Ganesan, A. L.: Rising atmospheric methane: 2007-2014 growth and isotopic shift, Global Biogeochemical Cycles, 30, 1356–1370, https://doi.org/10.1002/2016gb005406, 2016.

O'Dell, C. W., Connor, B., Bösch, H., O'Brien, D., Frankenberg, C., Castano, R., Christi, M., Eldering, D., Fisher, B., Gunson, M., McDuffie, J., Miller, C. E., Natraj, V., Oyafuso, F., Polonsky, I., Smyth, M., Taylor, T., Toon, G. C., Wennberg, P. O., and Wunch, D.: The ACOS CO_2 retrieval algorithm – Part 1: Description and validation against synthetic observations, Atmospheric Measurement Techniques, 5, 99–121, https://doi.org/10.5194/amt-5-99-2012, 2012.

Owor, M., Taylor, R., Mukwaya, C., and Tindimugaya, C.: Groundwater/surface-water interactions on deeply weathered surfaces of low relief: evidence from Lakes Victoria and Kyoga, Uganda, Hydrogeology Journal, 19, 1403–1420, https://doi.org/10.1007/s10040-011-0779-1, 2011.

Palmer, P. I.: The role of satellite observations in understanding the impact of El Niño on the carbon cycle: current capabilities and future opportunities, Phil. Trans. Roy. Soc. B, https://doi.org/10.1098/rstb.2017.0407, 2018.

Palmer, P. I., Feng, L., Baker, D., Chevallier, F., Bösch, H., and Somkuti, P.: Net carbon emissions from African biosphere dominate pan-tropical atmospheric CO2 signal, Nature Communications, 10, https://doi.org/10.1038/s41467-019-11097-w, 2019.

Pandey, S., Houweling, S., Krol, M., Aben, I., Chevallier, F., Dlugokencky, E. J., Gatti, L. V., Gloor, E., Miller, J. B., Detmers, R., Machida, T., and Röckmann, T.: Inverse modeling of GOSAT-retrieved ratios of total column CH_4 and CO_2 for 2009 and 2010, Atmospheric Chemistry and Physics, 16, 5043–5062, https://doi.org/10.5194/acp-16-5043-2016, 2016.

Parker, R., Boesch, H., Cogan, A., Fraser, A., Feng, L., Palmer, P. I., Messerschmidt, J., Deutscher, N., Griffith, D. W. T., Notholt, J., Wennberg, P. O., and Wunch, D.: Methane observations from the Greenhouse Gases Observing SATellite: Comparison to ground-based TCCON data and model calculations, Geophysical Research Letters, 38, https://doi.org/10.1029/2011gl047871, 2011.

Parker, R. J., Boesch, H., Byckling, K., Webb, A. J., Palmer, P. I., Feng, L., Bergamaschi, P., Chevallier, F., Notholt, J., Deutscher, N., Warneke, T., Hase, F., Sussmann, R., Kawakami, S., Kivi, R., Griffith, D. W. T., and Velazco, V.: Assessing 5 years of GOSAT Proxy XCH_4 data and associated uncertainties, Atmospheric Measurement Techniques, 8, 4785–4801, https://doi.org/10.5194/amt-8-4785-2015, 2015.

Parker, R. J., Boesch, H., McNorton, J., Comyn-Platt, E., Gloor, M., Wilson, C., Chipperfield, M. P., Hayman, G. D., and Bloom, A. A.: Evaluating year-to-year anomalies in tropical wetland methane emissions using satellite CH 4 observations, Remote Sensing of Environment, 211, 261–275, https://doi.org/10.1016/j.rse.2018.02.011, 2018.

Poulter, B., Bousquet, P., Canadell, J. G., Ciais, P., Peregon, A., Saunois, M., Arora, V. K., Beerling, D. J., Brovkin, V., Jones, C. D., Joos, F., Gedney, N., Ito, A., Kleinen, T., Koven, C. D., McDonald, K., Melton, J. R., Peng, C., Peng, S., Prigent, C., Schroeder, R., Riley, W. J., Saito, M., Spahni, R., Tian, H., Taylor, L., Viovy, N., Wilton, D., Wiltshire, A., Xu, X., Zhang, B., Zhang, Z., and Zhu, Q.: Global wetland contribution to 2000–2012 atmospheric methane growth rate dynamics, Environmental Research Letters, 12, 094 013, https://doi.org/10.1088/1748-9326/aa8391, 2017.

Prigent, C., Papa, F., Aires, F., Rossow, W. B., and Matthews, E.: Global inundation dynamics inferred from multiple satellite observations, 1993–2000, Journal of Geophysical Research, 112, https://doi.org/10.1029/2006jd007847, 2007.

Prigent, C., Papa, F., Aires, F., Jimenez, C., Rossow, W. B., and Matthews, E.: Changes in land surface water dynamics since the 1990s and relation to population pressure, Geophysical Research Letters, 39, n/a–n/a, https://doi.org/10.1029/2012gl051276, 2012.

Rebelo, L.-M., Senay, G. B., and McCartney, M. P.: Flood Pulsing in the Sudd Wetland: Analysis of Seasonal Variations in Inundation and Evaporation in South Sudan, Earth Interactions, 16, 1–19, https://doi.org/10.1175/2011ei382.1, 2012.

Rigby, M., Prinn, R. G., Fraser, P. J., Simmonds, P. G., Langenfelds, R. L., Huang, J., Cunnold, D. M., Steele, L. P., Krummel, P. B., Weiss, R. F., O'Doherty, S., Salameh, P. K., Wang, H. J., Harth, C. M., Mühle, J., and Porter, L. W.: Renewed growth of atmospheric methane, Geophysical Research Letters, 35, https://doi.org/10.1029/2008gl036037, 2008.

Rigby, M., Montzka, S. A., Prinn, R. G., White, J. W. C., Young, D., O'Doherty, S., Lunt, M. F., Ganesan, A. L., Manning, A. J., Simmonds, P. G., Salameh, P. K., Harth, C. M., Mühle, J., Weiss, R. F., Fraser, P. J., Steele, L. P., Krummel, P. B., McCulloch, A., and Park, S.: Role of atmospheric oxidation in recent methane growth, Proceedings of the National Academy of Sciences, 114, 5373–5377, https://doi.org/10.1073/pnas.1616426114, 2017.

Sanderson, M. G.: Biomass of termites and their emissions of methane and carbon dioxide: A global database, Global Biogeochemical Cycles, 10, 543–557, https://doi.org/10.1029/96gb01893, 1996.

Saunois, M., Bousquet, P., Poulter, B., Peregon, A., Ciais, P., Canadell, J. G., Dlugokencky, E. J., Etiope, G., Bastviken, D., Houweling, S., Janssens-Maenhout, G., Tubiello, F. N., Castaldi, S., Jackson, R. B., Alexe, M., Arora, V. K., Beerling, D. J., Bergamaschi, P., Blake, D. R., Brailsford, G., Brovkin, V., Bruhwiler, L., Crevoisier, C., Crill, P., Covey, K., Curry, C., Frankenberg, C., Gedney, N., Höglund-Isaksson, L., Ishizawa, M., Ito, A., Joos, F., Kim, H.-S., Kleinen, T., Krummel, P., Lamarque, J.-F., Langenfelds, R., Locatelli, R., Machida, T., Maksyutov, S., McDonald, K. C., Marshall, J., Melton, J. R., Morino, I., Naik, V., O'Doherty, S., Parmentier, F.-J. W., Patra, P. K., Peng, C., Peng, S., Peters, G. P., Pison, I., Prigent, C., Prinn, R., Ramonet, M., Riley, W. J., Saito, M., Santini, M., Schroeder, R., Simpson, I. J., Spahni, R., Steele, P., Takizawa, A., Thornton, B. F., Tian, H., Tohjima, Y., Viovy, N., Voulgarakis, A., van Weele, M., van der Werf, G. R., Weiss, R., Wiedinmyer, C., Wilton, D. J., Wiltshire, A., Worthy, D., Wunch, D., Xu, X., Yoshida, Y., Zhang, B., Zhang, Z., and Zhu, Q.: The global methane budget 2000–2012, Earth System Science Data, 8, 697–751, https://doi.org/10.5194/essd-8-697-2016, 2016.

Saunois, M., Bousquet, P., Poulter, B., Peregon, A., Ciais, P., Canadell, J. G., Dlugokencky, E. J., Etiope, G., Bastviken, D., Houweling, S., Janssens-Maenhout, G., Tubiello, F. N., Castaldi, S., Jackson, R. B., Alexe, M., Arora, V. K., Beerling, D. J., Bergamaschi, P., Blake, D. R., Brailsford, G., Bruhwiler, L., Crevoisier, C., Crill, P., Covey, K., Frankenberg, C., Gedney, N., Höglund-Isaksson, L., Ishizawa, M., Ito, A., Joos, F., Kim, H.-S., Kleinen, T., Krummel, P., Lamarque, J.-F., Langenfelds, R., Locatelli, R., Machida, T., Maksyutov, S., Melton, J. R., Morino, I., Naik, V., O'Doherty, S., Parmentier, F.-J. W., Patra, P. K., Peng, C., Peng, S., Peters, G. P., Pison, I., Prinn, R., Ramonet, M., Riley, W. J., Saito, M., Santini, M., Schroeder, R., Simpson, I. J., Spahni, R., Takizawa, A., Thornton, B. F., Tian, H., Tohjima, Y., Viovy, N., Voulgarakis, A., Weiss, R., Wilton, D. J., Wiltshire, A., Worthy, D., Wunch, D., Xu, X., Yoshida, Y., Zhang, B., Zhang, Z., and Zhu, Q.: Variability and quasi-decadal changes in the methane budget over the period 2000-2012, Atmospheric Chemistry and Physics, 17, 11 135–11 161, https://doi.org/10.5194/acp-17-11135-2017, 2017.

Schaefer, H., Fletcher, S. E. M., Veidt, C., Lassey, K. R., Brailsford, G. W., Bromley, T. M., Dlugokencky, E. J., Michel, S. E., Miller, J. B., Levin, I., Lowe, D. C., Martin, R. J., Vaughn, B. H., and White, J. W. C.: A 21st-century shift from fossil-fuel to biogenic methane emissions indicated by 13CH4, Science, 352, 80–84, https://doi.org/10.1126/science.aad2705, 2016.

Schroeder, R., McDonald, K., Chapman, B., Jensen, K., Podest, E., Tessler, Z., Bohn, T., and Zimmermann, R.: Development and Evaluation of a Multi-Year Fractional Surface Water Data Set Derived from Active/Passive Microwave Remote Sensing Data, Remote Sensing, 7, 16 688–16 732, https://doi.org/10.3390/rs71215843, 2015.

Sene, K. J.: Theoretical estimates for the influence of Lake Victoria on White Nile, Hydrological Sciences Journal, 45, https://doi.org/10.1080/02626660009492310, 2000.

Sosnowski, A., Ghoneim, E., Burke, J. J., Hines, E., and Halls, J.: Remote regions, remote data: A spatial investigation of precipitation, dynamic land covers, and conflict in the Sudd wetland of South Sudan, Applied Geography, 69, 51–64, https://doi.org/10.1016/j.apgeog.2016.02.007, 2016.

Sutcliffe, J. and Brown, E.: Water losses from the Sudd, Hydrological Sciences Journal, 63, 527–541, https://doi.org/10.1080/02626667.2018.1438612, https://doi.org/10.1080/02626667.2018.1438612, 2018.

Sutcliffe, J. V. and Parks, Y.: The Hydrology of the Nile, IAHS Spec. Publ, 1999.

Sutcliffe, J. V. and Petersen, G.: Lake Victoria: derivation of a corrected natural water level series /Lac Victoria: dérivation d'une série naturelle corrigée des niveaux d'eau, Hydrological Sciences Journal, 52, 1316–1321, https://doi.org/10.1623/hysj.52.6.1316, 2007.

Tapley, B. D., Bettadpur, S., Watkins, M., and Reigber, C.: The gravity recovery and climate experiment: Mission overview and early results, Geophysical Research Letters, 31, https://doi.org/10.1029/2004GL019920, 2004.

Tarantola, A.: Inverse Problem Theory and Methods for Model Paramenter Estimation, Cambridge University Press, http://www.ebook.de/de/product/12013271/albert_tarantola_inverse_problem_theory_and_methods_for_model_paramenter_estimation.html, 2005.

Tathy, J. P., Cros, B., Delmas, R. A., Marenco, A., Servant, J., and Labat, M.: Methane emission from flooded forest in central Africa, Journal of Geophysical Research, 97, 6159, https://doi.org/10.1029/90jd02555, 1992.

Taylor, C. M., Prigent, C., and Dadson, S. J.: Mesoscale rainfall patterns observed around wetlands in sub-Saharan Africa, Quarterly Journal of the Royal Meteorological Society, 144, 2118–2132, https://doi.org/10.1002/qj.3311, 2018.

Thompson, R. L., Nisbet, E. G., Pisso, I., Stohl, A., Blake, D., Dlugokencky, E. J., Helmig, D., and White, J. W. C.: Variability in Atmospheric Methane From Fossil Fuel and Microbial Sources Over the Last Three Decades, Geophysical Research Letters, 45, 11,499–11,508, https://doi.org/10.1029/2018gl078127, 2018.

Toit, C. D., Meissner, H., and Niekerk, W. V.: Direct methane and nitrous oxide emissions of South African dairy and beef cattle, South African Journal of Animal Science, 43, 320, https://doi.org/10.4314/sajas.v43i3.7, 2014.

Turner, A. J., Jacob, D. J., Wecht, K. J., Maasakkers, J. D., Lundgren, E., Andrews, A. E., Biraud, S. C., Boesch, H., Bowman, K. W., Deutscher, N. M., Dubey, M. K., Griffith, D. W. T., Hase, F., Kuze, A., Notholt, J., Ohyama, H., Parker, R., Payne, V. H., Sussmann, R., Sweeney, C., Velazco, V. A., Warneke, T., Wennberg, P. O., and Wunch, D.: Estimating global and North American methane emissions with high spatial resolution using GOSAT satellite data, Atmospheric Chemistry and Physics, 15, 7049–7069, https://doi.org/10.5194/acp-15-7049-2015, 2015.

Turner, A. J., Frankenberg, C., Wennberg, P. O., and Jacob, D. J.: Ambiguity in the causes for decadal trends in atmospheric methane and hydroxyl, Proceedings of the National Academy of Sciences, 114, 5367–5372, https://doi.org/10.1073/pnas.1616020114, 2017.

Turner, A. J., Frankenberg, C., and Kort, E. A.: Interpreting contemporary trends in atmospheric methane, Proceedings of the National Academy of Sciences, p. 201814297, https://doi.org/10.1073/pnas.1814297116, 2019.

van der Werf, G. R., Randerson, J. T., Giglio, L., van Leeuwen, T. T., Chen, Y., Rogers, B. M., Mu, M., van Marle, M. J. E., Morton, D. C., Collatz, G. J., Yokelson, R. J., and Kasibhatla, P. S.: Global fire emissions estimates during 1997–2016, Earth System Science Data, 9, 697–720, https://doi.org/10.5194/essd-9-697-2017, 2017.

Vanderkelen, I., van Lipzig, N. P. M., and Thiery, W.: Modelling the water balance of Lake Victoria (East Africa) – Part 1: Observational analysis, Hydrology and Earth System Sciences, 22, 5509–5525, https://doi.org/10.5194/hess-22-5509-2018, 2018.

Vittorio, C. A. D. and Georgakakos, A. P.: Land cover classification and wetland inundation mapping using MODIS, Remote Sensing of Environment, 204, 1–17, https://doi.org/10.1016/j.rse.2017.11.001, 2018.

Wecht, K. J., Jacob, D. J., Frankenberg, C., Jiang, Z., and Blake, D. R.: Mapping of North American methane emissions with high spatial resolution by inversion of SCIAMACHY satellite data, Journal of Geophysical Research: Atmospheres, 119, 7741–7756, https://doi.org/10.1002/2014jd021551, 2014.

Wolf, J., Asrar, G. R., and West, T. O.: Revised methane emissions factors and spatially distributed annual carbon fluxes for global livestock, Carbon Balance and Management, 12, https://doi.org/10.1186/s13021-017-0084-y, 2017.

Wolfe, G. M., Nicely, J. M., Clair, J. M. S., Hanisco, T. F., Liao, J., Oman, L. D., Brune, W. B., Miller, D., Thames, A., Abad, G. G., Ryerson, T. B., Thompson, C. R., Peischl, J., McKain, K., Sweeney, C., Wennberg, P. O., Kim, M., Crounse, J. D., Hall, S. R., Ullmann, K., Diskin, G., Bui, P., Chang, C., and Dean-Day, J.: Mapping hydroxyl variability throughout the global remote troposphere via synthesis of airborne and satellite formaldehyde observations, Proceedings of the National Academy of Sciences, 116, 11 171–11 180, https://doi.org/10.1073/pnas.1821661116, 2019.

Worden, J. R., Bloom, A. A., Pandey, S., Jiang, Z., Worden, H. M., Walker, T. W., Houweling, S., and Röckmann, T.: Reduced biomass burning emissions reconcile conflicting estimates of the post-2006 atmospheric methane budget, Nature Communications, 8, https://doi.org/10.1038/s41467-017-02246-0, 2017.

Wunch, D., Toon, G. C., Blavier, J.-F. L., Washenfelder, R. A., Notholt, J., Connor, B. J., Griffith, D. W. T., Sherlock, V., and Wennberg, P. O.: The Total Carbon Column Observing Network, Philosophical Transactions of the Royal Society A: Mathematical, Physical and Engineering Sciences, 369, 2087–2112, https://doi.org/10.1098/rsta.2010.0240, 2011.

Zhang, Z., Zimmermann, N. E., Calle, L., Hurtt, G., Chatterjee, A., and Poulter, B.: Enhanced response of global wetland methane emissions to the 2015–2016 El Niño-Southern Oscillation event, Environmental Research Letters, 13, 074 009, https://doi.org/10.1088/1748-9326/aac939, 2018.

Zimba, H., Kawawa, B., Chabala, A., Phiri, W., Selsam, P., Meinhardt, M., and Nyambe, I.: Assessment of trends in inundation extent in the Barotse Floodplain, upper Zambezi River Basin: A remote sensing-based approach, Journal of Hydrology: Regional Studies, 15, 149–170, https://doi.org/10.1016/j.ejrh.2018.01.002, 2018.

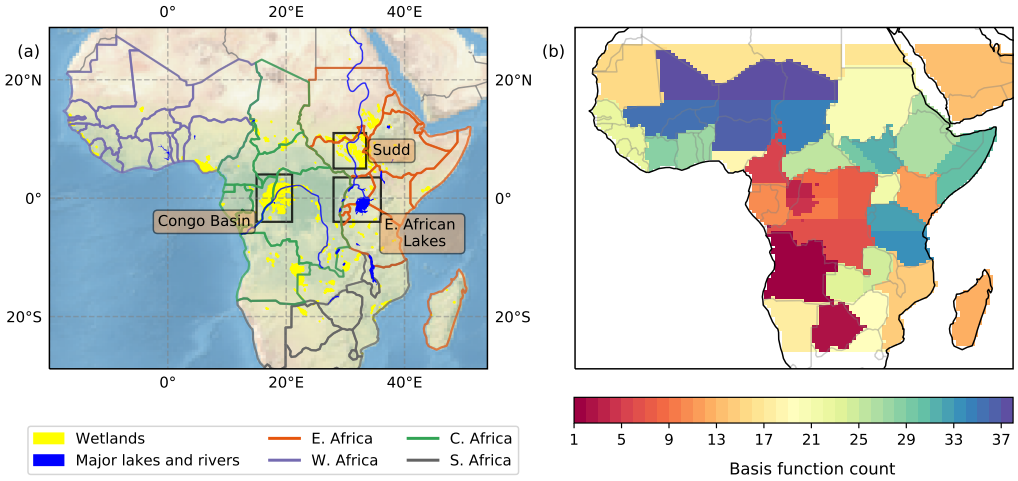

Figure 1. (a) Map of our tropical African model domain. Wetland regions from Gumbricht et al. (2017) are marked in yellow and major rivers and lakes are marked in blue. The Congo Basin, the Sudd, and the East African Lakes are outlined by black boxes. The division into regions of the African Union are shown by the different colour country borders, indicating Central Africa (green), East Africa (orange), Southern Africa (grey) and West Africa (purple). The map background represents shaded relief from https://www.naturalearthdata.com; (b) The spatial emission basis functions used in our inversions.

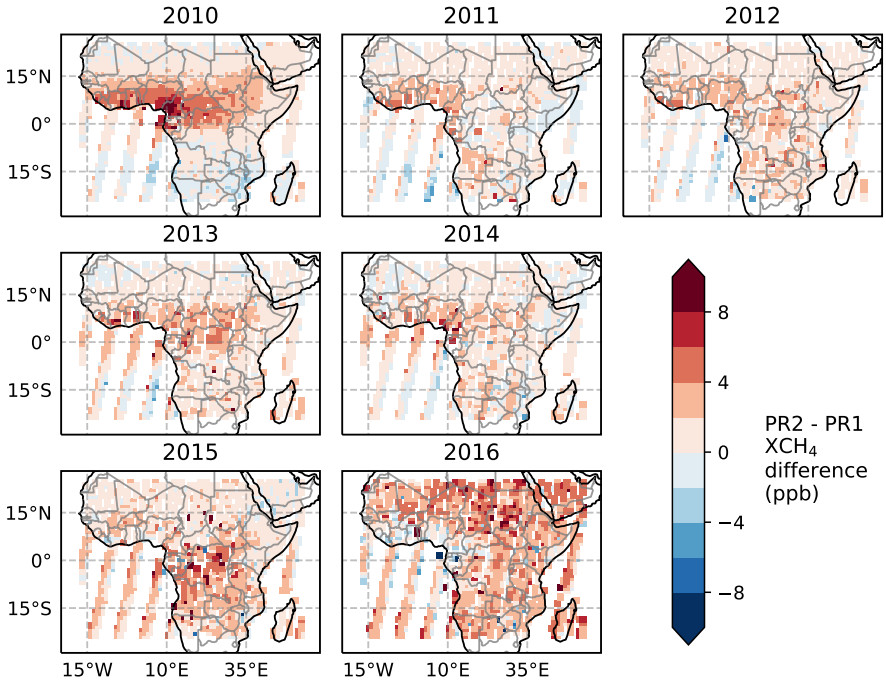

Figure 2. Annual mean differences between PR1 and PR2 proxy XCH_4 data at 1°x1° resolution. PR1 represents the data from Parker et al. (2015). PR2 uses our own $CO_{2\ model}$ component, generated from an inversion of GOSAT XCO_2 data to form the proxy XCH_4 data.

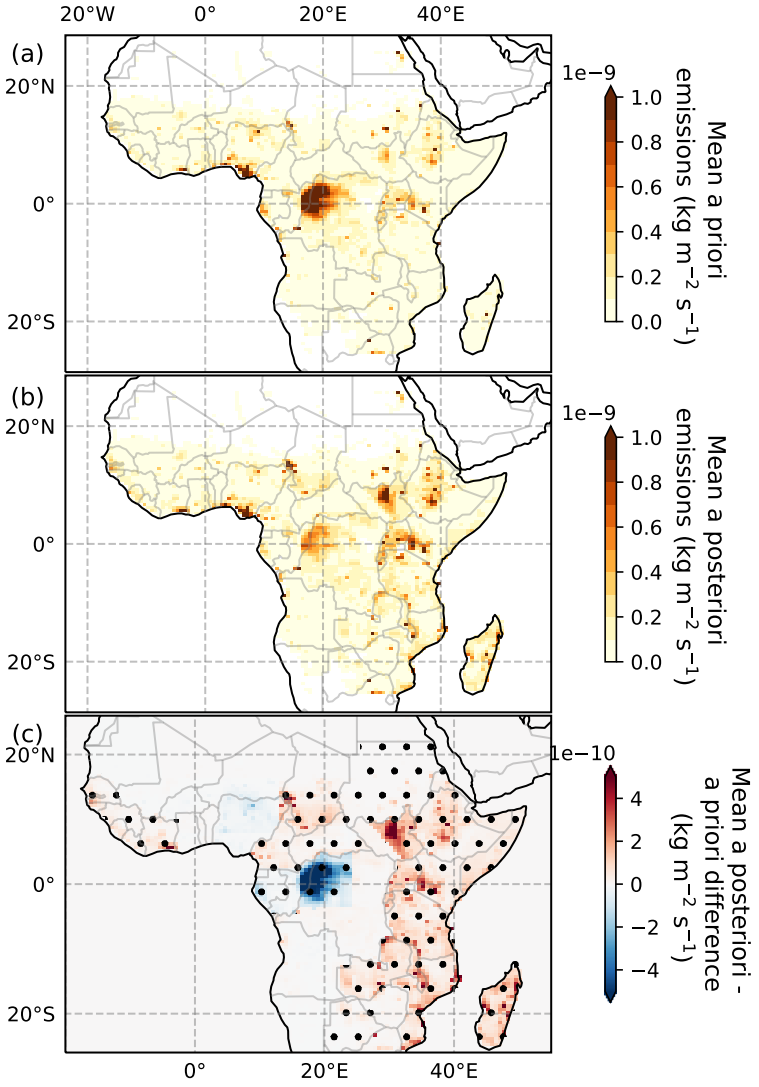

Figure 3. The 2010–2016 mean (a) *a priori* and (b) *a posteriori* spatial distribution of CH_4 emissions in the tropical African domain from the PR1 inversion. (c) Mean PR1 *a posteriori* minus *a priori* differences, 2010–2016. Stippling indicates areas where the *a priori* mean was outside the *a posteriori* 95% uncertainty range for both PR1 and PR2 inversions.

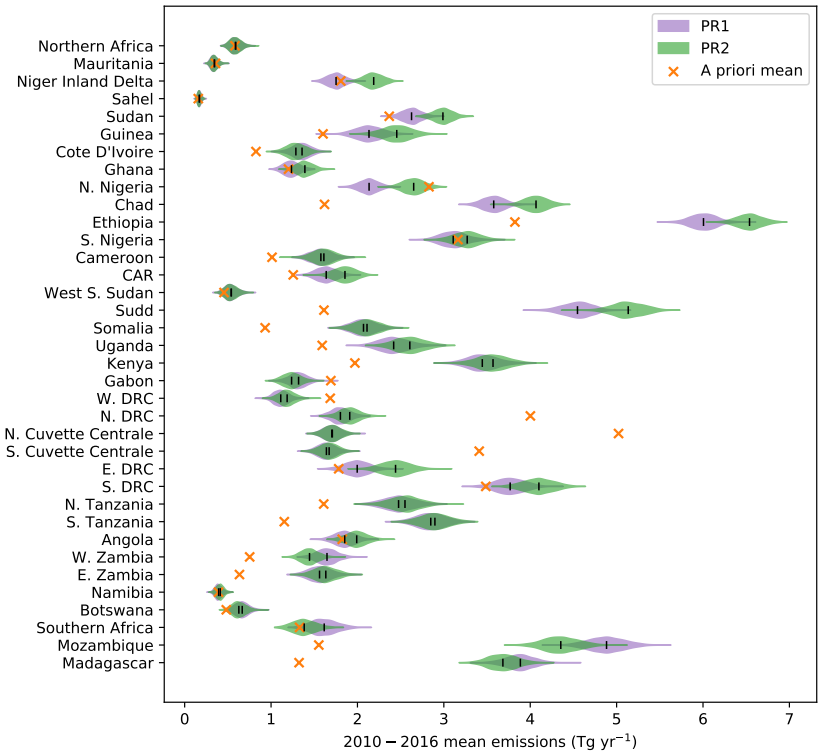

Figure 4. Violin plot of the *a posteriori* distribution from each African basis function for the PR1 (purple) and PR2 (green) inversions over 2010–2016. The lines in the centre of the violins represent the mean of each respective distribution. The *a priori* mean value for each basis function region is shown by the orange cross. Basis function regions are ordered from South to North travelling up the y-axis. The region names on the y-axis are intended to be representative of the respective regions and not necessarily an exact definition based on country borders. CAR is the Central African Republic. DRC is the Democratic Republic of Congo.

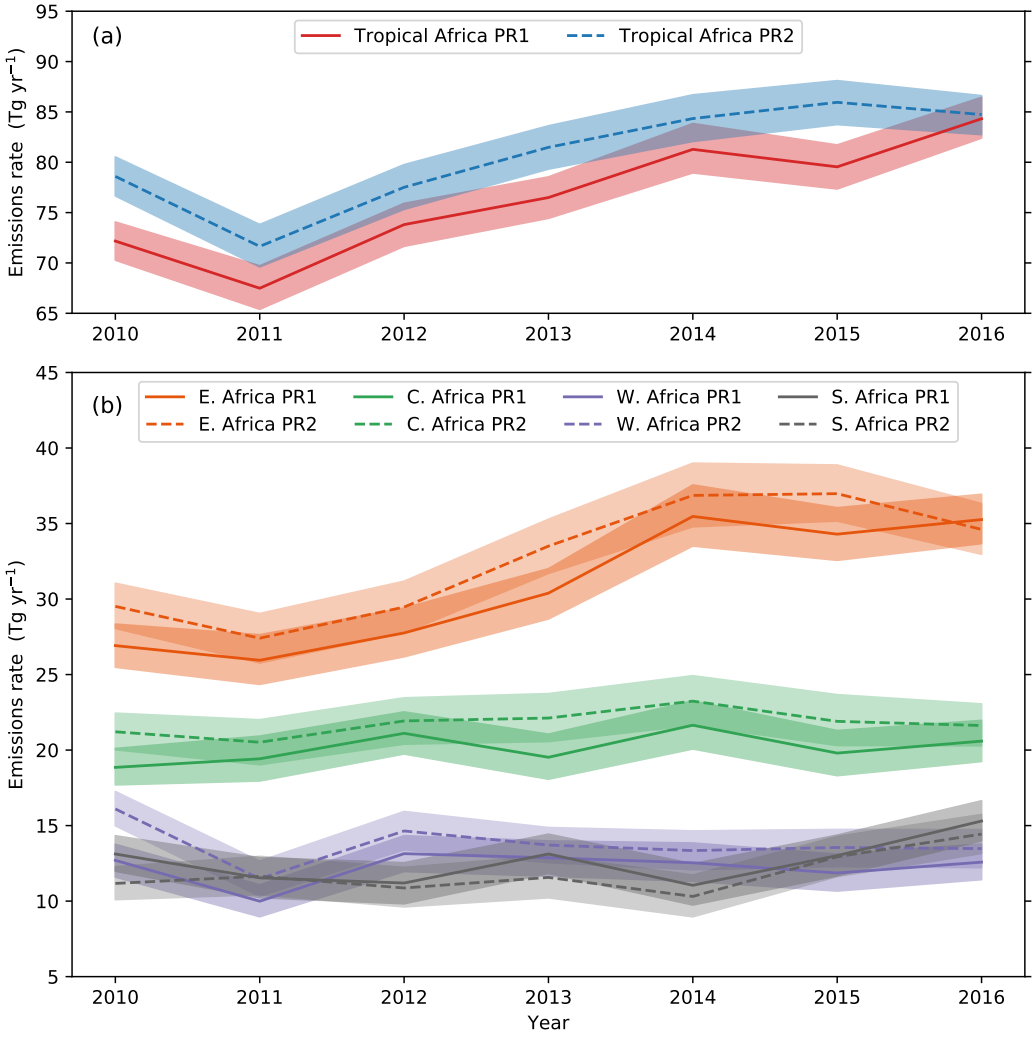

Figure 5. (a) Annual *a posteriori* emissions for tropical Africa. (b) Annual *a posteriori* emissions for East Africa (blue), Central Africa (purple), West Africa (orange) and Southern Africa (grey). Solid lines represent the PR1 *a posteriori* mean, dashed lines indicate the PR2 *a posteriori* mean in each panel. Shading represents the 95% uncertainty range in both panels.

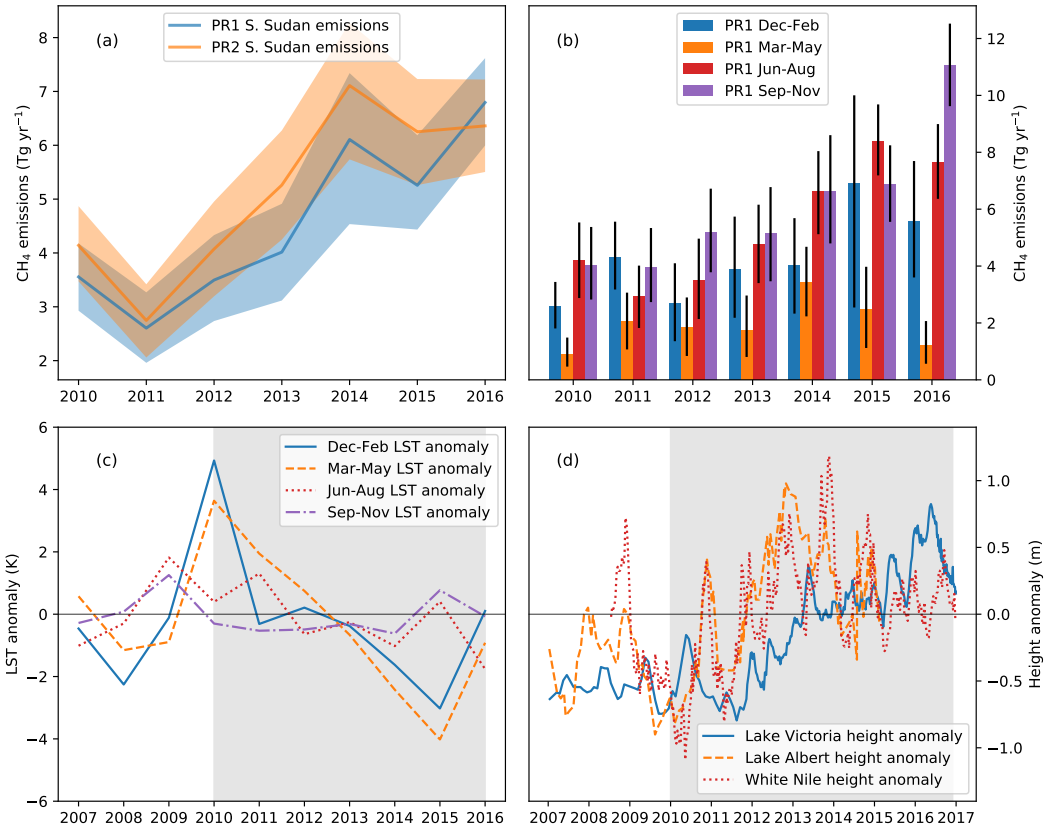

Figure 6. (a) Annual mean *a posteriori* emissions from the area encompassing the Sudd in South Sudan from PR1 (blue) and PR2 (orange) inversions. Shading represents the 95% uncertainty range. (b) The annual mean of Sudd emissions in each season from the PR1 inversions. Uncertainty bars represent the 95% uncertainty range. (c) The annual mean LST anomaly in each season from the Sudd, used as a proxy for wetland extent between 2007–2016. Negative anomalies indicate increased soil moisture. The grey shading indicates the inversion period when the decrease in LST anomalies occurs. (d) Satellite altimetry data from Lake Victoria (blue), Lake Albert (orange) and the White Nile at 6.55 °N, 31.40 °E (red) between 2007–2016, showing the transient increase in upstream water levels during the inversion period (grey shading).

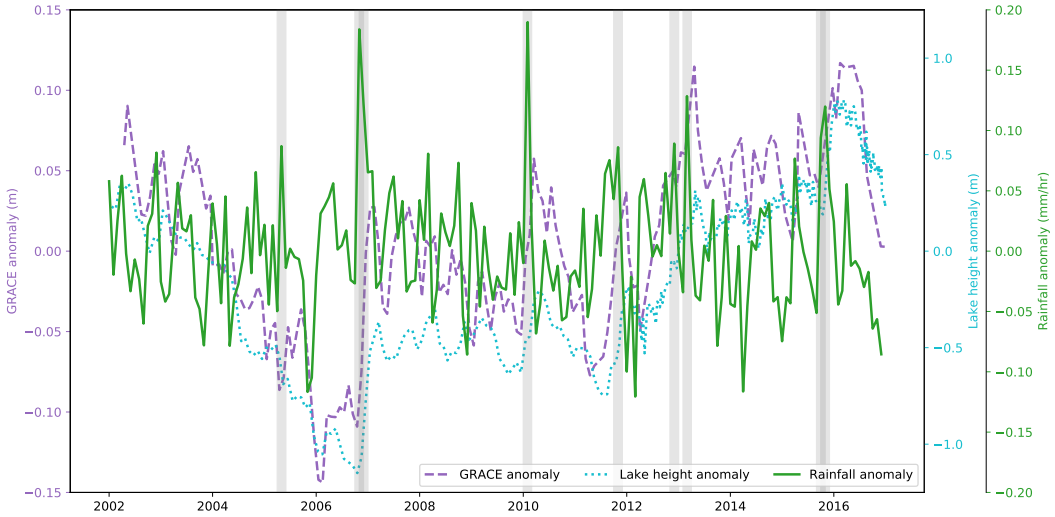

Figure 7. Monthly anomalies of precipitation over the Lake Victoria basin from the Tropical Rainfall Measuring Mission (TRMM, green), GRACE LWE over the basin (purple) and Lake Victoria water height (cyan). Anomalies represent the departures from the mean of each month between 2002–2016, to remove seasonal cycle influence. Grey shading indicates 3-month periods centred on months where the precipitation anomaly was greater than the 95th percentile. These periods coincide with rises in both LWE and lake height anomalies, highlighting the role of heavy rainfall on lake level increases.

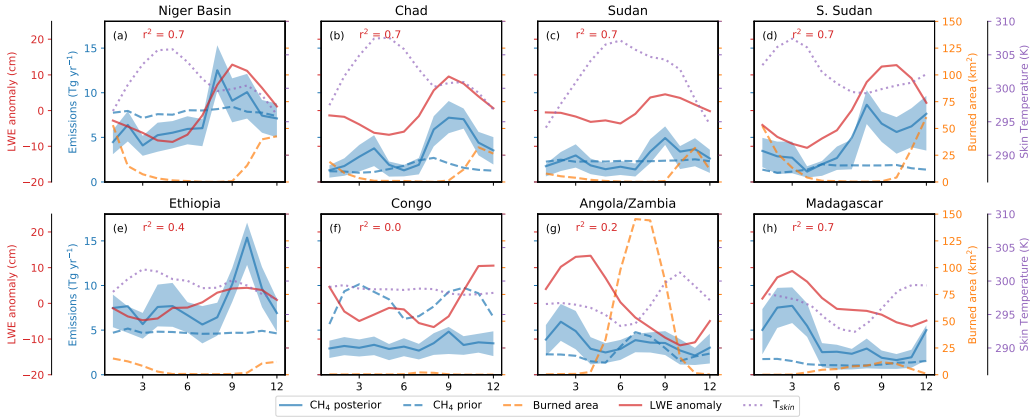

Figure 8. Mean seasonal cycle of *a posteriori* CH_4 (solid blue) emissions from eight regions across tropical Africa. Shading represents the 95% uncertainty range. Also shown are the *a priori* emissions (dashed blue), burned area (orange dashes), GRACE liquid water equivalent height anomaly (LWE, red), and surface skin temperature (T_{skin}) estimates from MERRA-2 (purple dots). Plots (a)–(e) represent regions in northern hemisphere Africa with CH_4 emissions peak in the latter part of the year and (g)–(h) are in southern hemisphere Africa where the CH_4 emission peak is at the start of the year. (f) Congo straddles the equator. The r^2 value represents the correlation coefficient between *a posteriori* emissions and LWE values.